Arteriosclerosis, Thrombosis, and Vascular Biology

JOURNAL OF THE AMERICAN HEART ASSOCIATION

Loss of *CDKN2B* Promotes p53-Dependent Smooth Muscle Cell Apoptosis and Aneurysm Formation

Nicholas J. Leeper, Azad Raiesdana, Yoko Kojima, Ramendra K. Kundu, Henry Cheng, Lars Maegdefessel, Ryuji Toh, G-One Ahn, Ziad A. Ali, D. Ryan Anderson, Clint L. Miller, Scott C. Roberts, Joshua M. Spin, Patricia E. de Almeida, Joseph C. Wu, Baohui Xu, Karen Cheng, Maximilian Quertermous, Soumajit Kundu, Kim E. Kortekaas, Erica Berzin, Kelly P. Downing, Ronald L. Dalman, Philip S. Tsao, Eric E. Schadt, Gary K. Owens and Thomas Quertermous

Arterioscler Thromb Vasc Biol. 2013;33:e1-e10; originally published online November 15, 2012;
doi: 10.1161/ATVBAHA.112.300399
Arteriosclerosis, Thrombosis, and Vascular Biology is published by the American Heart Association, 7272 Greenville Avenue, Dallas, TX 75231

Print ISSN: 1079-5642. Online ISSN: 1524-4636

Loss of *CDKN2B* Promotes p53-Dependent Smooth Muscle Cell Apoptosis and Aneurysm Formation

Nicholas J. Leeper,* Azad Raiesdana,* Yoko Kojima, Ramendra K. Kundu, Henry Cheng, Lars Maegdefessel, Ryuji Toh, G-One Ahn, Ziad A. Ali, D. Ryan Anderson, Clint L. Miller, Scott C. Roberts, Joshua M. Spin, Patricia E. de Almeida, Joseph C. Wu, Baohui Xu, Karen Cheng, Maximilian Quertermous, Soumajit Kundu, Kim E. Kortekaas, Erica Berzin, Kelly P. Downing, Ronald L. Dalman, Philip S. Tsao, Eric E. Schadt, Gary K. Owens, Thomas Quertermous

Objective—Genomewide association studies have implicated allelic variation at 9p21.3 in multiple forms of vascular disease, including atherosclerotic coronary heart disease and abdominal aortic aneurysm. As for other genes at 9p21.3, human expression quantitative trait locus studies have associated expression of the tumor suppressor gene *CDKN2B* with the risk haplotype, but its potential role in vascular pathobiology remains unclear.

Methods and Results—Here we used vascular injury models and found that *Cdkn2b* knockout mice displayed the expected increase in proliferation after injury, but developed reduced neointimal lesions and larger aortic aneurysms. In situ and in vitro studies suggested that these effects were attributable to increased smooth muscle cell apoptosis. Adoptive bone marrow transplant studies confirmed that the observed effects of *Cdkn2b* were mediated through intrinsic vascular cells and were not dependent on bone marrow–derived inflammatory cells. Mechanistic studies suggested that the observed increase in apoptosis was attributable to a reduction in MDM2 and an increase in p53 signaling, possibly due in part to compensation by other genes at the 9p21.3 locus. Dual inhibition of both *Cdkn2b* and p53 led to a reversal of the vascular phenotype in each model.

Conclusion—These results suggest that reduced *CDKN2B* expression and increased smooth muscle cell apoptosis may be one mechanism underlying the 9p21.3 association with aneurysmal disease. (***Arterioscler Thromb Vasc Biol*. 2013;33:e1-e10.**)

Key Words: abdominal aortic aneurysm ■ apoptosis ■ CDKN2B ■ genomewide association studies ■ p53 ■ remodeling ■ smooth muscle

As much as half of the risk for atherosclerotic coronary heart disease (CHD) is genetic in nature.[1,2] Through genomewide association studies, ≈30 loci have now been associated with CHD.[3,4] To date, the most robust genomewide association finding for CHD is a group of highly correlated variants in an ≈58 kilobase region on chromosome 9 at p21.3, the chromosome 9p21.3 CHD-Associated Region (C9CAR).[5,6] C9CAR has been associated with atherosclerosis burden and myocardial infarction,[4,7,8] as well as extracardiac phenotypes such as abdominal aortic aneurysm (AAA), peripheral arterial disease, and stroke.[9–12] As much as 20% of the attributable risk for CHD is contributed by variation at C9CAR.[5] The simultaneous association of 9p21.3 variation with nonatherosclerotic berry aneurysms suggests that the unifying mechanisms of association may not occur via a classical inflammatory pathway, but rather through some process that governs the structural makeup of the diseased vessel wall.[11]

To date, the causal gene(s) at 9p21.3 remain unclear. The closest genes to C9CAR include a group of 3 cancer-related factors that reside over 50 kilobases telomeric to the risk associated region. Two of these genes, *CDKN2A* and *CDKN2B*, are cyclin-dependent kinase inhibitors that interact with CDK4 and CDK6 and have been linked to cell cycle regulation. The third is a unique splice variant of *CDKN2A* termed *p14/ARF* that is involved in regulation of apoptosis through interactions with p53.[13] All of these genes are considered tumor suppressors and are commonly silenced by methylation in a

Received on: August 30, 2012; final version accepted on: October 31, 2012.

From the Departments of Surgery (N.J.L., B.X., K.E.K., K.P.D., R.L.D.) and Medicine (A.R., Y.K., R.K.K., H.C., L.M., R.T., G-O.A., Z.A.A., D.R.A., C.L.M., S.C.R., J.M.S., P.E.d.A., J.C.W., K.C., M.Q., S.K., P.S.T., T.Q.), Stanford University School of Medicine, Stanford, CA; Department of Research, Pacific Biosciences, Menlo Park, CA (E.E.S.); and Robert M. Berne Cardiovascular Research Center, University of Virginia School of Medicine, Charlottesville, VA (E.B., G.K.O.).

*These authors contributed equally to this work.

The online-only Data Supplement is available with this article at http://atvb.ahajournals.org/lookup/suppl/doi:10.1161/ATVBAHA.112.300399/-/DC1.

Correspondence to Thomas Quertermous, MD, Division of Cardiovascular Medicine, Stanford University, 300 Pasteur Dr, Stanford, CA 94305. E-mail tomq1@stanford.edu

variety of cancers.[13,14] Both *CDKN2A* and *CDKN2B* have been implicated in biological processes such as senescence, apoptosis, stem cell renewal, and adult onset diabetes mellitus.[13] *CDKN2A* and *ARF* have been linked to CHD through gene expression and animal models of experimental atherosclerosis,[15–17] but no study has yet examined the effects of genes near 9p21 on aneurysm formation. Because several recent genetics-of-gene-expression studies have associated C9CAR variants with altered expression of *CDKN2B*[17–20] (and/or its antisense long noncoding RNA, *ANRIL*),[20,21] we used a series of in vitro and in vivo murine vascular disease models to investigate the mechanisms by which *CDKN2B* might regulate heritable vascular risk, with a particular focus on AAA disease.

Methods

Murine Vascular Disease Models

All animal protocols used were approved by the Stanford University Administrative Panel on Laboratory Animal Care. All experiments were performed in 12- to 14-week-old male *Cdkn2b*$^{+/+}$ (n=107) and *Cdkn2b*$^{-/-}$ (n=85) mice on a C57BL/6 background.

Negative vascular remodeling was induced by performing complete carotid artery ligation (CAL). In some experiments, mice were injected with 2.2 mg/kg IP pifithrin-α 1 hour before ligation, and then every 48 hours until sacrifice, as above. Animals were euthanized 2, 4, 7, 14, or 28 days after the surgery and both the ligated and nonligated carotid artery samples were harvested for either RNA, total protein, or histomorphometric analysis as described in the online-only Data Supplement Methods.

Porcine pancreatic elastase infusion was used to generate aortic aneurysms. Abdominal aortic diameter was measured at baseline and 7 and 14 days after aneurysm induction, with B-mode ultrasound imaging. In some experiments, mice were injected with 2.2 mg/kg IP pifithrin-α 1 day before surgery, and then every 48 hours until being euthanized. Animals were euthanized 5 or 14 days after surgery, and analyzed as described in the online-only Data Supplement Methods.

Reciprocal bone marrow transplant studies were performed in lethally irradiated mice, as described in the online-only Data Supplement Methods. After 14 days of recovery, engraftment was confirmed by flow cytometry and the mice were subjected to porcine pancreatic elastase infusion, as above.

Human Vascular Sample Acquisition and Preparation

Human aortic samples were taken from patients during open surgical AAA repair (n=13), or from organ donors at the time of explant (n=5) and subjected to quantitative real-time reverse transcriptase polymerase chain reaction mRNA expression analysis. Immunohistochemical analyses were performed on aneurysmal (n=7) and nonaneurysmal aortic sections (n=7) from a second confirmation cohort.

Cell Culture Methods

Human coronary, pulmonary, and aortic smooth muscle cells (SMC; Lonza) were grown in media provided by the supplier. Endothelial cells, monocytes, macrophages, and fibroblasts were studied as described in the online-only Data Supplement Methods. To induce growth arrest and the expression of differentiation genes, SMC were serum starved in basal media for 72 hours. In vitro p53 inhibition studies were done by adding 10 μmol/L pifithrin-α (Calbiochem) to the cell culture media. For knockdown experiments, human coronary artery SMC (HCASMC) were transfected with 300 nmol/L of anti-*CDKN2B* or high-GC negative control small interfering RNA (Ambion) using the Amaxa Nucleofector system (Lonza).

Cellular proliferation was quantified with a modified (3-[4,5-dimethylthiazol-2-yl]-2,5-diphenyltetrazolium bromide) (MTT) assay as well as cell counting and fluorescence-activated cell sorter (FACS) analysis. To analyze SMC migration, a modified Boyden chamber assay was performed.

Rates of programmed cell death were assessed with 3 independent in vitro assays. In each assay, 1×10^5 transfected HCASMC were treated with 1 μmol/L staurosporine (Sigma) in serum-free media for 6 hours before analysis. Caspase-3 and -7 activity was measured using a commercially available luminometric assay (Promega). In the second assay, the cells were FACS sorted for fluorescein isothiocyanate annexin V and propidium iodide (BD FACSCaliber). In the final assay, cells were fixed in 10% formalin before terminal deoxynucleotidyl transferase dUTP nick end labeling staining with the Cell Death Detection Kit (Roche).

Phosphoproteomic antibody microarray profiling and bioinformatics analyses were performed in *CDKN2B*-deficient cells, as described in the online-only Data Supplement Methods.

Expression Analysis

Standard methodology was applied for mRNA and protein extraction from cell lysates and vascular samples, as well as for subsequent gene expression analysis and Western blotting, as described in the online-only Data Supplement Methods.

Statistical Analysis

Data are presented as mean±SEM. Data were subjected to the Kolmogorov-Smirnov test to determine distribution. Groups were compared using the Mann-Whitney *U* test for nonparametric data or the Students *t* test for parametric data. When comparing multiple groups, data were analyzed by analysis of variance with Bonferroni post-test. Statistical analysis was performed with GraphPad Prism 5.

Additional Methods

Detailed methodology and primary citations are provided in the online-only Data Supplement Methods.

Results

Cdkn2b Regulates Both Negative Vascular Remodeling and Aneurysm Formation In Vivo

To investigate the impact of a loss of *Cdkn2b* in vivo, we studied the CAL injury model and the elastase-infusion AAA model in *Cdkn2b*$^{-/-}$ and *Cdkn2b*$^{+/+}$ mice. No difference in blood pressure, heart rate, lipid level, or glucose level was observed between genotypes (Figure I in the online-only Data Supplement).

In the CAL model, *Cdkn2b*$^{-/-}$ mice exhibited reduced neointimal areas (41.4% reduction, $P<0.03$), medial areas (10.0% reduction, $P<0.03$), and intimal-to-medial ratios (37.2% reduction, $P<0.05$) compared with control *Cdkn2b*$^{+/+}$mice 4 weeks after vascular injury (Figure 1A). No measurable differences in luminal area ($P=0.24$) or total vessel area ($P=0.15$) were observed. *Cdkn2b*$^{-/-}$ mice displayed accelerated dropout of SMC and had less vascular smooth muscle α-actin staining than *Cdkn2b*$^{+/+}$ animals (31.6% reduction, $P<0.03$), as well as fewer total neointimal cells, as assessed by number of 4′,6-diamidino-2-phenylindole-positive nuclei (212.9 fewer cells/vessel, $P<0.03$; Figure 1B and 1C).

In the AAA model, *Cdkn2b*$^{-/-}$ mice were found to develop significantly larger aortic aneurysms than *Cdkn2b*$^{+/+}$control mice at both the 1 week (44.4% larger, $P<0.01$) and 2 week (29.3% larger, $P<0.01$) time points after elastase infusion (Figure 1E). In keeping with the CAL model findings above, *Cdkn2b*$^{-/-}$ mice had significantly less smooth muscle α-actin staining (46.0% reduction, $P<0.05$; Figure 1F). No significant

differences in elastin degradation score (P=0.23; Figure 1G), Mac-3 (P=0.24), CD-3 (P=0.87), or collagen staining (P=0.92) were observed between genotypes (data not shown).

In both models, the *Cdkn2b*$^{-/-}$ mice displayed increased cellular proliferation in response to vessel injury. In the CAL model, significant differences were observed 1 week (3.81-fold increase, P<0.01) and 4 weeks (5.65-fold increase, P<0.0001; Figure 1D) after ligation. In the AAA model, there was a marked increase in proliferation 5 days after elastase infusion (1.66-fold increase, P<0.01; Figure 1H) as measured by the number of proliferating cell nuclear antigen-positive vascular cells.

Cdkn2b Mediates Its Effects Through Resident Vascular Cells Independent of Bone Marrow–Derived Cells

To confirm that *Cdkn2b* was mediating its effect solely through intrinsic blood vessel cells and not via an inflammatory mechanism, we next performed elastase infusions in mice that had been lethally irradiated and that had undergone adoptive bone marrow transplantation (Figure II in the online-only Data Supplement). *Cdkn2b*$^{-/-}$ mice reconstituted with wild-type marrow developed significantly larger AAAs than *Cdkn2b*$^{+/+}$ mice that had been reconstituted with either *Cdkn2b*$^{-/-}$ or *Cdkn2b*$^{+/+}$ marrow (176.9% versus 155.1% and 145.8% aortic diameter increase, respectively, P<0.05; Figure 2A). Only the *Cdkn2b*$^{-/-}$ recipients displayed a reduction in smooth muscle α-actin staining, confirming an effect of this gene on resident SMC survival (58.0% reduction relative to *Cdkn2b*$^{+/+}$/*Cdkn2b*$^{+/+}$ mice, P<0.03). No difference in T cell or macrophage infiltrate was observed across genotypes in either the CAL or elastase model (P=NS for each, data not shown).

Cdkn2b Regulates Vascular Disease In Vivo by Inhibiting Programmed Cell Death

To explain how the knockout animals could have enhanced proliferation yet develop smaller neointimal lesions and aneurysms with fewer SMC, we next evaluated the rates of apoptosis in each genotype. The *Cdkn2b*$^{-/-}$ mice in the CAL model displayed a striking increase in apoptosis observed as early as 2 days after injury (3.32-fold increase, P<0.03; Figure 2B) that

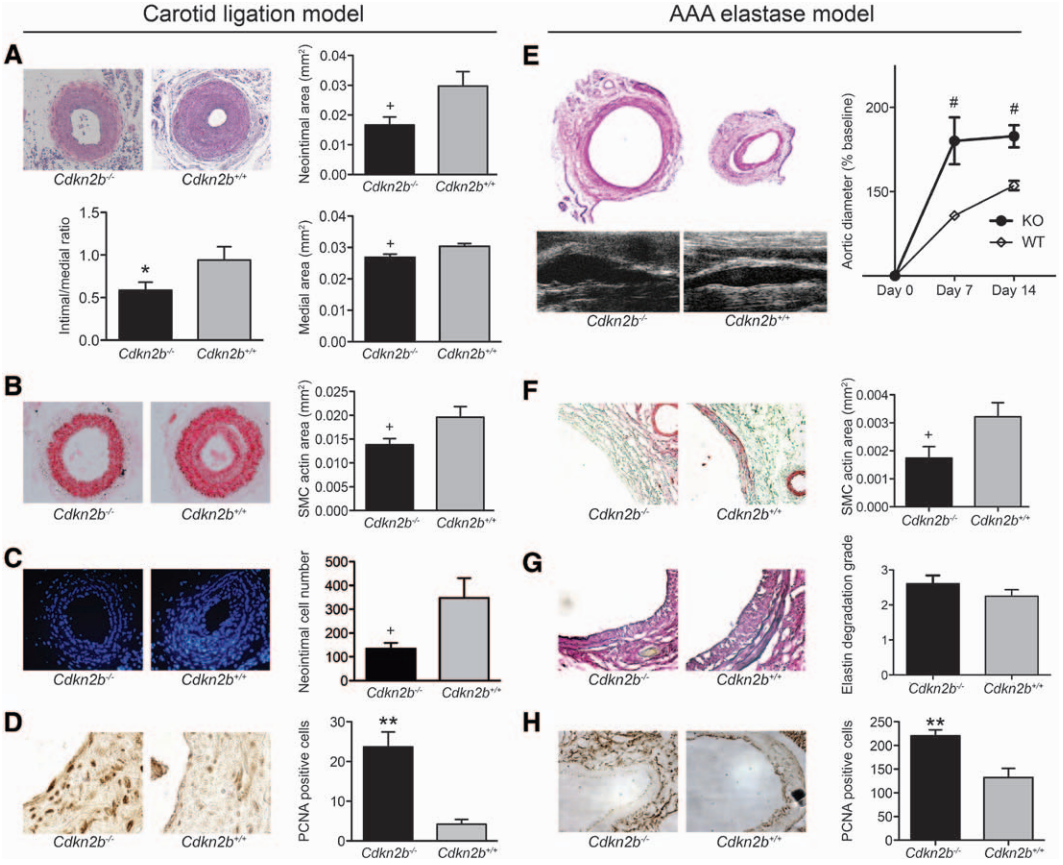

Figure 1. *Cdkn2b* regulates murine vascular disease. **A**, *Cdkn2b*$^{-/-}$ mice display alterations in vascular remodeling in the carotid ligation model 28 days after vascular injury. Compared with *Cdkn2b*$^{+/+}$ mice (**right**, n=15), *Cdkn2b*$^{-/-}$ mice (**left**, n=19) have smaller neointimal areas (**upper right**), medial areas (**lower right**), and intimal-to-medial ratios (**lower left**). **B**, *Cdkn2b*$^{-/-}$ vessels have less smooth muscle cell (SMC) content as measured by SMC α-actin positive area, and (**C**) fewer total vascular cells as assessed by number of 4',6-diamidino-2-phenylindole (DAPI) positive nuclei. **D**, *Cdkn2b*$^{-/-}$ mice displayed higher rates of cell division as assessed by proliferating cell nuclear antigen (PCNA) stain. **E**, *Cdkn2b*$^{-/-}$ mice (n=9) also develop significantly larger aortic aneurysms in the elastase infusion model than *Cdkn2b*$^{+/+}$ mice (n=8), with (**F**) associated decrease in SMC number, and no significant difference in (**G**) elastin degradation score. **H**, As in the carotid artery ligation (CAL) model, there was a significant increase in cell proliferation in aortas of elastase model *Cdkn2b*$^{-/-}$ mice. *P<0.05; +P<0.03; #P<0.01; **P<0.001.

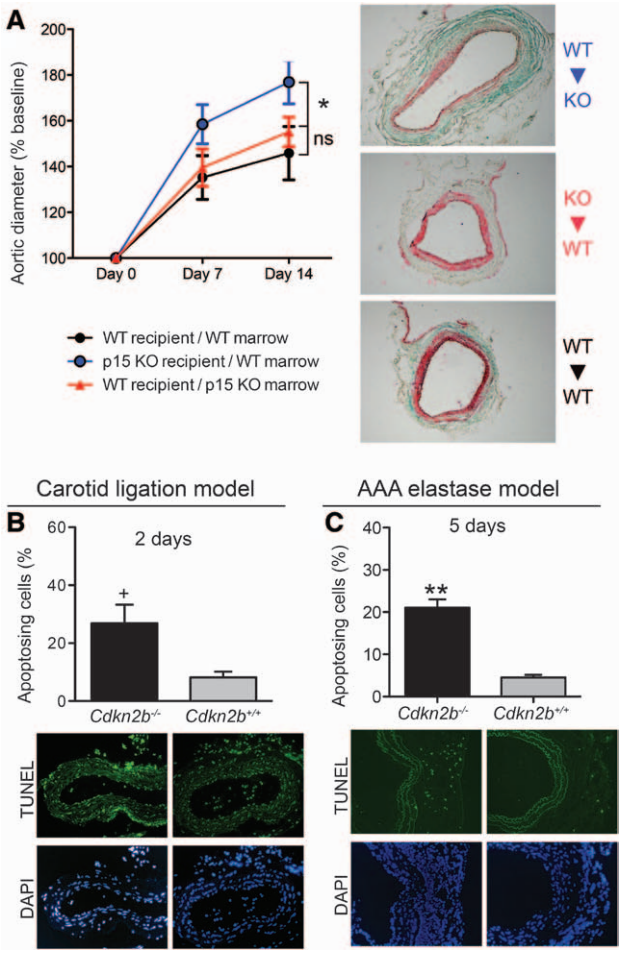

Figure 2. *Cdkn2b* regulates apoptosis in vivo and potentiates disease through intrinsic vessel wall cells. **A**, Bone marrow transplant studies revealed that the vascular effects of *Cdkn2b* are not mediated through bone marrow–derived cells, with enhanced aneurysms only observed in the $Cdkn2b^{-/-Recipient}/WT^{Donor}$ group compared with the $WT^{Recipient}/Cdkn2b^{-/-Donor}$ and $WT^{Recipient}/WT^{Donor}$ groups (n=15 in each group, $P<0.05$). Similarly, a significant reduction in smooth muscle cell (SMC) α-actin content was only observed in the $Cdkn2b^{-/-Recipient}$ group. **B**, $Cdkn2b^{-/-}$ mice (n=8) displayed markedly elevated rates of vascular apoptosis relative to $Cdkn2b^{+/+}$ mice (n=8) 2 days after ligation (3.32-fold increase, $P<0.03$), as assessed by percentage of terminal deoxynucleotidyl transferase dUTP nick end labeling (TUNEL)-positive cells in the remodeling carotid artery. These differences were no longer observed 4 weeks after vascular injury. **C**, $Cdkn2b^{-/-}$ mice (n=9) displayed increased aortic apoptosis relative to $Cdkn2b^{+/+}$mice (n=5) 5 days after elastase infusion (4.64-fold increase, $P<0.0001$) in the abdominal aortic aneurysm (AAA) model.

persisted 1 week postligation (1.96-fold increase, $P<0.05$). Also, the $Cdkn2b^{-/-}$ mice displayed increased aortic apoptosis relative to $Cdkn2b^{+/+}$ mice 5 days after elastase infusion (4.64-fold increase, $P<0.0001$) in the AAA model (Figure 2C). In each model, the differences were no longer observed at the terminal time point, several weeks after injury ($P>0.22$ for each).

CDKN2B Is Expressed in Vascular SMC and Is Downregulated in Diseased Vascular Tissue

To define the localization of *CDKN2B* in human vascular tissue and understand its regulation in vascular disease, we investigated the expression of *CDKN2B* in normal and pathological vascular samples. Compared with explants from organ donors, aortic samples taken from patients undergoing open AAA repair showed markedly reduced *CDKN2B* mRNA levels (4.8-fold reduction, $P<0.03$; Figure IIIA in the online-only Data Supplement). Similarly, studies revealed that *Cdkn2b* expression was decreased in an animal model of vascular injury, with a 3-fold reduction observed in murine carotid arterial tissue 2 weeks after carotid ligation ($P<0.01$). In keeping with these findings, we found that *CDKN2B* was expressed at a high level in cultured SMC at baseline (in contrast to cultured endothelial cells and macrophages) and was significantly downregulated as cells assumed the dedifferentiated phenotype (7.2-fold reduction, $P<0.01$).

Immunolocalization of *CDKN2B*-expressing cells was performed with human aortic sections from a separate AAA cohort, and confirmed that *CDKN2B* was highly expressed in medial vascular SMCs in vivo, but decreased in aneurysm tissue (Figure IIIB in the online-only Data Supplement). Semiquantitative analysis of these data confirmed the mRNA expression findings, revealing that *CDKN2B* was highly downregulated in aneurysmal compared with nonaneurysmal tissue ($P<0.01$). Further staining in human vascular sections revealed colocalization of *CDKN2B* and smooth muscle α-actin staining. Colocalization of *CDKN2B* and von Willebrand factor expression was present but less intense (Figure IIIC in the online-only Data Supplement).

CDKN2B Regulates Proliferation, Migration, and Apoptosis in Cultured SMC

Given findings implicating the tunica media as the site of action of *CDKN2B,* we next evaluated the role of this gene in vascular SMC physiology in vitro. HCASMC were rendered deficient in *CDKN2B* through treatment with small interfering RNA (10.5-fold knockdown, $P<0.01$). These cells revealed a significantly higher rate of proliferation than control-transfected cells, as measured using an MTT assay (0.028 versus 0.019 relative proliferation units, $P<0.01$, Figure 3A) and hemocytometer cell counts (25.9% increase, $P<0.03$). Consistent with these findings, cells deficient in *CDKN2B* were also found to have higher rates of mitosis by FACS analysis, as evidenced by a higher frequency of G2/M phase cells (4.6 versus 3.5%, $P<0.01$; Figure 3B). Also, small interfering RNA–induced suppression of *CDKN2B* was associated with significant enhancement of SMC migration in Boyden chamber assays (15.4 versus 9.6 cells/hpf, $P<0.0001$; Figure 3C). In keeping with the in vivo data, *CDKN2B* was then also found to inhibit programmed cell death using 3 independent assays. Both the percentage of terminal deoxynucleotidyl transferase dUTP nick end labeling-stained apoptotic cells grown on chamber slides (38.5 versus 13.2%, $P<0.01$, Figure 3D) and the caspase-3/7 activity (13 414 versus 6715 relative light units, $P<0.0001$; Figure 3E) were significantly increased in *CDKN2B*-deficient cells relative to control cells. Similarly, *CDKN2B* knockdown increased the percentage of cells stained for annexin V compared with control-transfected cells (65.8 versus 46.3%, $P<0.05$) after exposure to the proapoptotic global kinase inhibitor staurosporine (Figure 3F). These apoptotic differences were confirmed in human aortic SMC ($P<0.01$, data not shown). *CDKN2B* was not expressed in cultured macrophages, did not modulate

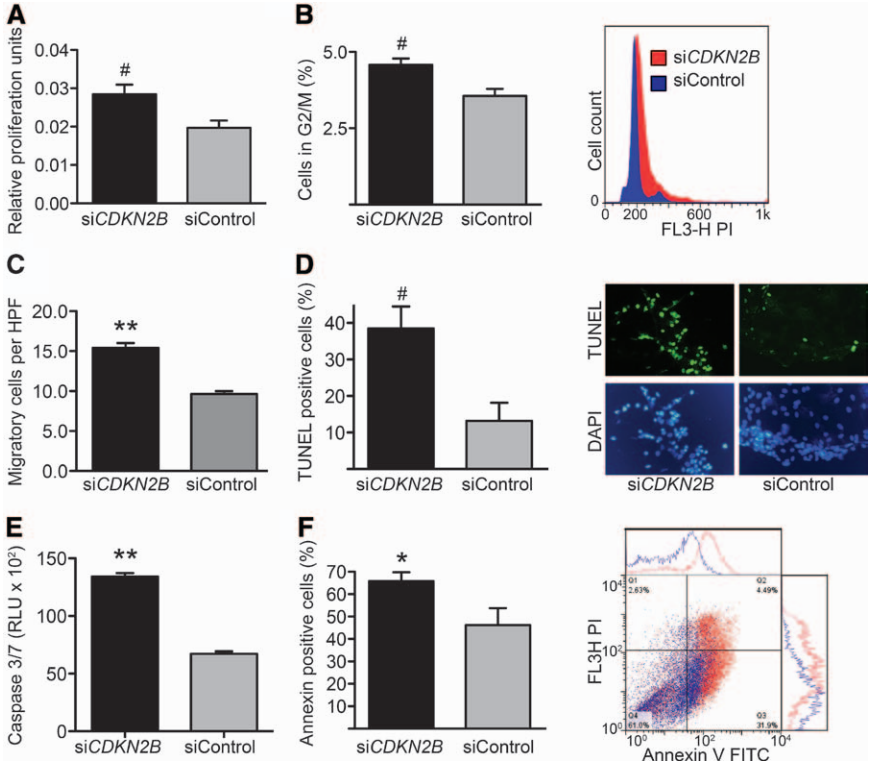

Figure 3. *CDKN2B* regulates smooth muscle cell (SMC) functions in cultured human vascular smooth muscle cells. HCASMC deficient in *CDKN2B* (*siCDKN2B*) have higher rates of proliferation than control cells (*si*Control) as assessed by (**A**) (3-[4,5-dimethylthiazol-2-yl]-2,5-diphenyltetrazolium bromide) (MTT) assay and (**B**) percentage of cells in G2/M phase by fluorescence-activated cell sorter (FACS) analysis. **C**, *siCDKN2B*-treated cells have higher rates of migration in the Boyden chamber assay than *si*Control cells. *siCDKN2B*-treated cells have significantly higher rates of programmed cell death, as assessed by (**D**) terminal deoxynucleotidyl transferase dUTP nick end labeling (TUNEL) staining in chamber slides, (**E**) Caspase 3/7 activity, and (**F**) annexin V positivity by FACS analysis, confirming the in vivo findings.

monocyte differentiation, and did not regulate apoptosis in cultured fibroblasts (P=NS, data not shown). Knockdown of *CDKN2B* had no measurable effect on the expression of SMC-differentiation markers (Figure IV in the online-only Data Supplement), inflammatory cytokines, or extracellular matrix collagens in SMC (P=NS for each, data not shown).

9p21 Genes Are Regulated in Response to Stress

Because compensatory back-up roles have been described for genes at the 9p21 locus previously,[14] we next evaluated the expression of each of the genes near C9CAR in response to stress. A pattern of reduced CDKN2B with increased CDKN2A and Arf expression was observed both in vitro and in vivo after injury (control cells treated with an apoptotic stimuli (grey bars, Figure 4A) and wild-type carotid tissue after ligation (grey bars, Figure 4B). MTAP fell after injury in vivo, but not in vitro. When evaluating the changes which occurred during conditions of CDKN2B-deficiency, a similar pattern was observed (compare black bars with grey bars in Figure 4A and 4B), with the exception of Cdkn2a which was elevated in knockout mice at baseline and did not augment in response to stress. A direct comparison of the relative responses to stress across genotypes revealed a significantly larger increase in the proapoptotic factor alternate reading frame (Arf) in *Cdkn2b*$^{-/-}$ mice compared with *Cdkn2b*$^{+/+}$ mice after carotid injury (P<0.05; Figure 4B) but only a trend in vitro (P=0.07). The relative compensation of all other 9p21-locus genes was similar across genotypes (P>0.05 for each).

CDKN2B Regulates SMC Apoptosis via an MDM2 and p53-Dependent Mechanism

To further investigate the mechanism by which *CDKN2B* regulates SMC survival, we next evaluated the expression of apoptosis-regulating genes in HCASMC lacking *CDKN2B* and in the injured vessel wall of CAL mice lacking *Cdkn2b*. Western blot analysis revealed that *CDKN2B* knockdown in HCASMC resulted in increased expression of p53 (2.9-fold increase, P<0.03) and its downstream product p21 (3.7-fold increase, P<0.05) as compared with control-transfected cells (Figure 4C). These differences were associated with a concomitant increase in the proapoptotic factor Bcl-2 associated protein (Bax) (6.3-fold increase, P=0.18) and a decrease in the antiapoptotic factor BCL2 (1.8-fold decrease, P=0.056), although these changes did not reach statistical significance. Modulation of *CDKN2B* in vitro did not significantly alter total retinoblastoma protein levels (1.9-fold increase, P=0.11). In the CAL model, *Cdkn2b*$^{-/-}$ mice showed a significant increase in *Trp53* (2.8-fold increase, P<0.03), *p21* (3.1-fold increase, P<0.05), *p19/Arf* (2.8-fold increase, P<0.03) and *Bax* (2.2-fold increase, P<0.03), with a nonsignificant decrease in *Bcl2* mRNA expression relative to *Cdkn2b*$^{+/+}$ ligated vessels, confirming the cell-based findings (Figure 4D).

To further study the mechanism by which a deficiency in *CDKN2B* resulted in enhanced p53 expression, we performed a phospho-antibody protein microarray analysis of 196 factors related to the p53 signaling and apoptotic pathways. Intensity signals representing protein levels in apoptosing *CDKN2B*-deficient and control-transfected cells were evaluated with Significance Analysis of Microarrays, and the genes responsible for differentially regulated proteins (false discovery rate <1%) were evaluated by overabundance analysis using the Database for Annotation Visualization and Integrated Discovery (DAVID) (P<0.05, 2 genes/category minimum). Enriched Kyoto Encyclopedia of Genes and Genomes (KEGG) pathways revealed that *CDKN2B* regulates genes related to SMC function, cell cycling, malignancy, and, as predicted, the p53 pathway

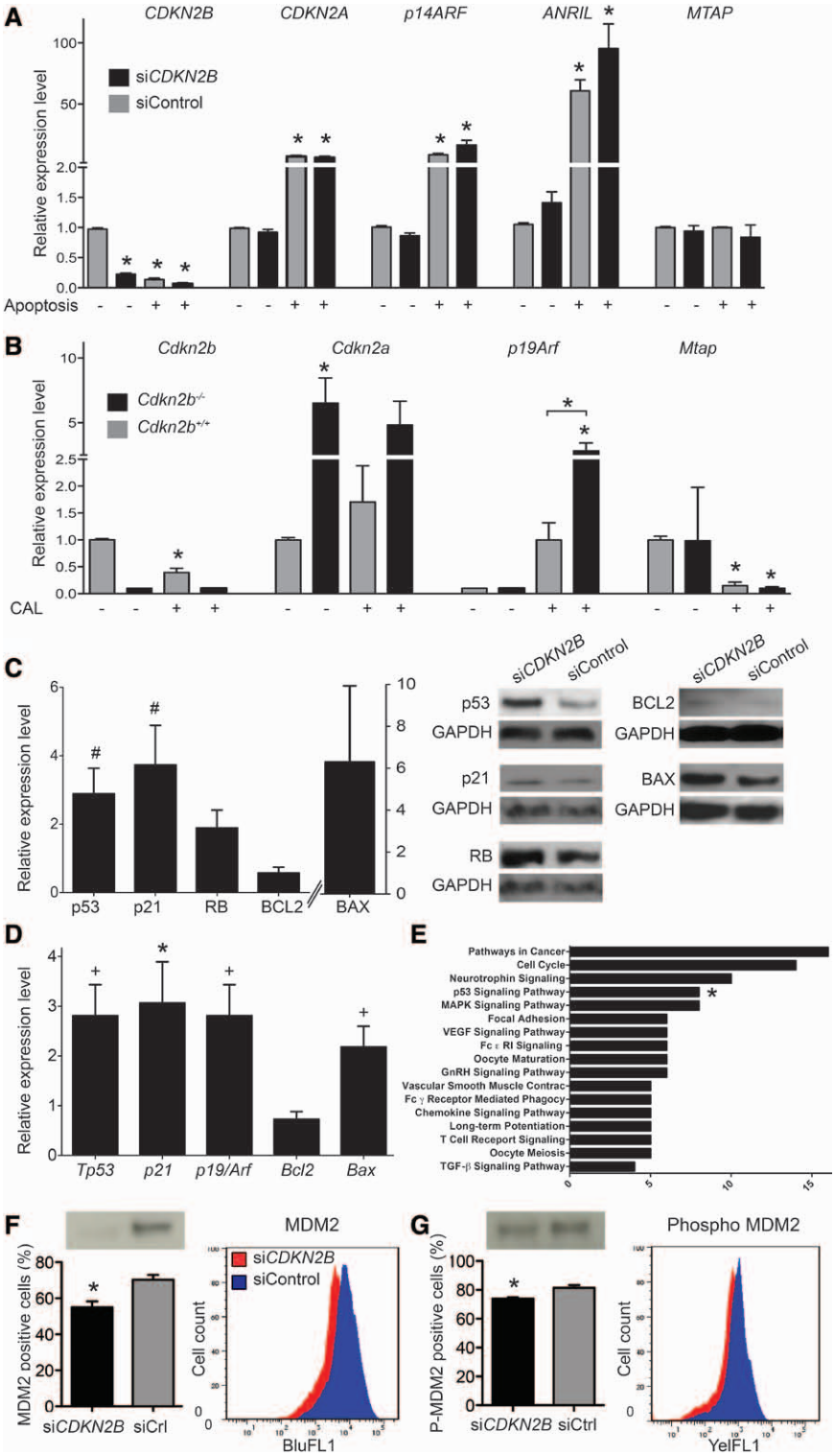

Figure 4. Compensation occurs at the 9p21 locus in response to stress and loss of *CDKN2B* promotes the activity of apoptotic factors, including MDM2 and p53. **A**, In response to an apoptotic stimulus, control-transfected HCASMC (grey bars) display reduced expression of *CDKN2B* and increased expression of *CDKN2A, ARF,* and *ANRIL*. A similar pattern is observed in *CDKN2B*-deficient cells (black bars). All comparisons are made with basal, control-transfected cells (*P<0.05). **B**, A similar pattern of compensation is observed in carotid tissue in vivo in wild-type mice (n=7, grey bars) after carotid injury. Comparing the relative response to stress in *Cdkn2b*$^{-/-}$ mice (n=7, black bars) reveals that the change in Arf is accentuated compared with wild-type animals (P<0.05). **C**, Western blot analysis of apoptosing *CDKN2B*-deficient HCASMC also revealed a significant upregulation of p53 and the downstream p21 protein relative to control small interfering RNA (siRNA) transfected cells. A trend toward increased expression of the proapoptotic protein BAX and reduced expression of the antiapoptotic protein BCL-2 was also observed. Retinoblastoma (RB) expression was not significantly changed by knockdown of *CDKN2B*. Quantitative densitometric data are shown in graph format on the **left**, representative blots with GAPDH loading controls on the **right**. **D**, mRNA expression analysis of mouse carotid tissue 4 days after carotid ligation confirm the in vitro findings, with significant upregulation of *Trp53*, *p21*, *Arf,* and *Bax* observed in the vessels of *Cdkn2b*$^{-/-}$ mice (n=7) relative to *Cdkn2b*$^{+/+}$ mice (n=7). **C**, Phospho-antibody protein microarray studies and Kyoto Encyclopedia of Genes and Genomes (KEGG) analysis in HCASMC confirm the central role of the p53 apoptotic pathway in *CDKN2B* signaling. Among the differentially regulated genes annotated under the p53 signaling pathway (asterisks), MDM2 was the most significantly altered. Flow cytometry assays and Western blot analyses confirmed the protein array data and reveal that apoptotic *CDKN2B*-deficient HCASMC express significantly less total MDM2 than apoptotic control-transfected cells (**D**, P<0.01) as well as phosphorylated MDM2 (**E**, P<0.01).

(Figure 4E). Interestingly, the MDM2 protein was the third most significantly regulated candidate on the array (ahead of p53 itself), suggesting that *CDKN2B* may regulate apoptosis by targeting an MDM2-stabilizing kinase to enhance p53 ubiquitination and degradation. Subsequent flow cytometry and Western blot studies confirmed the array-based findings and revealed that apoptosing *CDKN2B*-deficient cells expressed significantly lower levels of both total MDM2 and phospho-MDM2 than control-transfected cells, explaining the higher levels of p53 in the knockdown cells (P<0.01 for each; Figure 4F and 4G).

Dual Inhibition Studies Confirm the Role of p53 in CDKN2B-Mediated Apoptosis and Vascular Remodeling

Finally, to determine whether the observed *CDKN2B*-related apoptotic differences were dependent on p53 signaling, we

performed dual targeting studies that included the pharmacological p53 inhibitor, pifithrin-α. Simultaneous knockdown of p53 augmented the enhanced proliferation in *CDKN2B* deficient HCASMC based on FACS analyses, with the ratio of cells in G2/M increasing from 1.28 at baseline to 1.66 after pifithrin-α treatment (Figure 5A). In contrast, inactivation of p53 eliminated the difference in apoptosis between *CDKN2B* knockdown and control-transfected cells, as assessed by caspase 3/7 activity, terminal deoxynucleotidyl transferase dUTP nick end labeling staining, and FACS analysis of annexin V positivity (Figure 5B–5D). *Cdkn2b*$^{-/-}$ mice administered pifithrin-α parenterally no longer showed increased rates of apoptosis after carotid ligation (Figure 5E) and actually exhibited a reversal of the remodeling phenotype after CAL, with an increase in the ratio of neointimal areas and intimal:medial ratios (Figure 5F). Similar results were observed in the AAA model, where the rate of aneurysm expansion was no longer different between genotypes after pifithrin-α treatment (P>0.71 at each time point; Figure 5G).

Discussion

The present study provides a hypothesis for how *CDKN2B* might contribute to heritable cardiovascular risk. The data suggest that it does so, at least in part, by inducing multiple functional alterations in vascular SMC that could impact disease development, progression, and end stage clinical consequences. First, we show that reduced *Cdkn2b* expression in murine vascular remodeling and AAA models accelerates SMC proliferation while paradoxically leading to both smaller neointimal lesions and larger aortic aneurysms. Second, we show that these changes are secondary to an increase in vascular apoptosis, which is the result of an interaction between *CDKN2B* and the MDM2-p53 pathway, possibly attributable at least in part to upregulation of ARF in the presence of vascular injury. These *CDKN2B*-related effects on programmed cell death appear to be the major determinant of the observed vascular phenotype, have the capacity to overwhelm the concomitant proliferative differences, occur through an effect on resident vascular cells, and can be fully reversed by simultaneously inhibiting both the p53 and *CDKN2B* pathways. Although further investigation is required in additional models, these studies suggest one mechanism for how a gene which is regulated by polymorphisms at C9CAR may potentiate risk for AAA.[5,22]

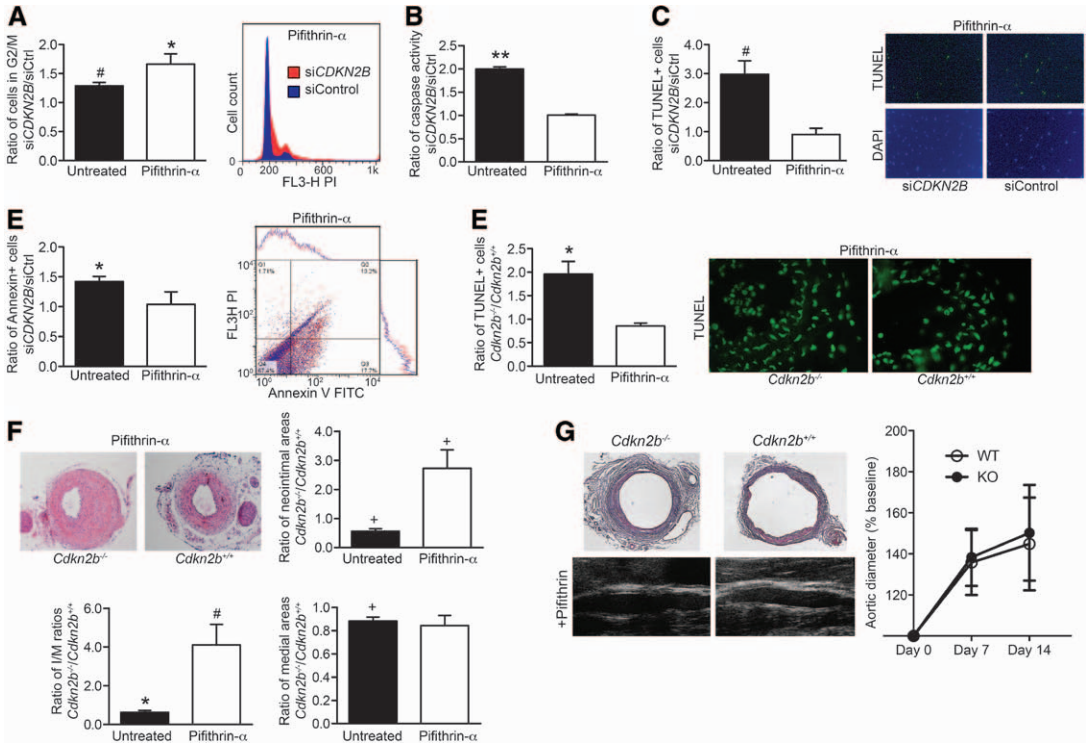

Figure 5. The effects of *CDKN2B* on remodeling and apoptosis are dependent on p53. In vitro, inhibition of both *CDKN2B* and p53 eliminated the difference in apoptosis while enhancing the difference in proliferation. **A**, Inhibition of p53 with pifithrin-α accentuated the ratio of cell proliferation in *CDKN2B* deficient HCASMC relative to control-transfected cells (si*CDKN2B*/siCtrl) compared with the baseline ratio. In contrast, treatment with pifithrin-α eliminated the difference in staurosporine-induced apoptosis that was noted at baseline, as assessed by (**B**) caspase 3/7 activity, (**C**) terminal deoxynucleotidyl transferase dUTP nick end labeling (TUNEL) positivity, and (**D**) annexin-V positivity by fluorescence-activated cell sorter (FACS) analysis. In vivo, *p53* inhibition also neutralized the difference in apoptosis between *Cdkn2b*$^{-/-}$ (n=6) and *Cdkn2b*$^{+/+}$ mice (n=7) and led to a reversal of the remodeling phenotype compared with baseline. **E**, One week after carotid ligation, the ratio of TUNEL-positive cells between the *Cdkn2b*$^{-/-}$ and *Cdkn2b*$^{+/+}$ genotypes (*Cdkn2b*$^{-/-}$/*Cdkn2b*$^{+/+}$) had normalized in mice treated with IP pifithrin-α, compared with baseline where the knockout mice had nearly double the rate of apoptosis (n=5 for each). **F**, Four weeks after ligation, *Cdkn2b*$^{-/-}$ mice treated with intraperitoneal pifithrin-α had larger neointimal areas and intimal:medial (I/M) ratios than wild-type mice also treated with the p53 inhibitor, showing a reversal of phenotype after inhibiting the p53 pathway. **G**, Similarly, aneurysm expansion was no longer different between genotypes after pifithrin-α treatment, (P>0.7) at each time point (n=6 vs 5).

The identity of the causal vascular disease gene(s) at 9p21 remains the topic of significant debate. To date, a number of expression quantitative trait locus and allelic imbalance studies have been performed in human tissues, and altered expression of each of the genes (alone or in combination) near the 9p21 locus has been described in carriers of the risk allele, including *CDKN2A, ARF, ANRIL,* and *MTAP*.[17,20,21,23,24] For *CDKN2B*, expression quantitative trait locus studies have associated noncoding C9CAR risk single-nucleotide polymorphisms with reduced *CDKN2B* expression in man, including adipose tissue and circulating leukocytes.[4,17] Importantly, recent studies have extended these mapping efforts into vascular tissue and found reduced *CDKN2B* expression in atherosclerotic plaque and vascular SMCs derived from carriers of the risk allele, consistent with association in the end organ.[18,19] At a mechanistic level, much of the observed reduction in *CDKN2B* expression may be occurring indirectly through the local long noncoding RNA, *ANRIL,* which has been shown to epigenetically suppress *CDKN2B* transcription,[25,26] and has been associated with C9CAR allelic variation.[20,21,23] Indeed, a recent study revealed that a lead C9CAR polymorphism ablates a STAT1 binding site in a 9p21 enhancer element, resulting in enhanced *ANRIL* expression, and presumably reduced *CDKN2B* in the vessel wall.[27] Finally, recent association studies in Americans of African ancestry have identified risk variants within the *CDKN2B* 3′-untranslated region,[28] and one of these variants has now been independently associated in a large meta-analysis of 63 746 CHD cases and 130 681 controls by the CARDIoGRAM+C4D consortium (CARDIoGRAMplusC4D C, submitted, 2012).

The observation that *CDKN2B* is strongly linked to SMC apoptosis may explain the association of 9p21 with both AAA disease and nonatherosclerotic intracranial aneurysms. A central feature of these diseases, and for berry aneurysms in particular, is a decrease in vascular wall integrity related to loss of vascular wall medial SMC number.[29] Aneurysmal dilatation has also been associated with SMC apoptosis and p53 upregulation in human aneurysms.[30] For carriers of the C9CAR risk haplotype, pathological downregulation of *CDKN2B* would enhance p53-dependent apoptosis, and ultimately promote medial thinning. Because vascular SMC turnover occurs at an exceedingly low rate,[31] it is possible that even a slight imbalance in the ratio of proliferation to apoptosis might have a dramatic impact on AAA progression, particularly when considered over a period of several decades.[32,33]

An important point is that the effects observed here are mediated solely through intrinsic vessel-wall cells, and not bone marrow–derived macrophages. This consideration is important given that previous studies have implicated *Cdkn2b* in monocytic myeloproliferation[34] and previous observations that most cardiovascular diseases are inflammatory in nature.[32] However, the link between risk haplotype and the nonatherosclerotic berry aneurysm points to a mechanism that governs blood vessel composition over one that promotes vascular inflammation. Indeed, this hypothesis was borne out by our observation that the *Cdkn2b* knockout mice displayed a severe phenotype in each animal model, with no increase in inflammatory cell burden, as well as a null effect after transplanting knockout marrow into otherwise healthy animals. The fact that *Cdkn2b* does not alter vascular inflammation may explain its independence from classical risk factors such as smoking, dyslipidemia, and diabetes mellitus, as these processes appear to primarily work through inflammatory pathways, rather than medial cell fate decision making.[35]

Apoptosis-related signaling downstream of *CDKN2B* appears to be more complex than previously appreciated. In health, both *CDKN2B* and *CDKN2A* are well described inhibitors of tumor formation that signal through the retinoblastoma pathway to inhibit the G_1 to S transition. In human cancer, these 2 genes are coordinately hypermethylated or deleted, allowing tumor growth.[13,14] In the vasculature, *CDKN2B* similarly regulates cell fate decisions, but appears to have an even greater role in the modulation of apoptosis in response to stress. Rather than doing so through the retinoblastoma pathway, a loss of *CDKN2B* results in activation of the p53 axis and several downstream effector molecules. p53 has been implicated in vascular remodeling previously,[36] but its role in atherosclerotic plaque progression is the subject of significant debate.[37,38] There are several possible mechanisms by which signaling between *CDKN2B* and p53 may occur (Figure IV in the online-only Data Supplement). In keeping with extensive literature linking ARF to p53, one possible mechanism identified through these studies is the upregulation of vascular ARF expression in response to reduced *CDKN2B* expression. These data would suggest that either direct modulation of ARF by causal variation at C9CAR, or indirect modulation of ARF through intermediate regulation of *CDKN2B* could provide a common disease pathway. An argument against a sole role for ARF in the context of *CDKN2B* downregulation is provided by data obtained in an Arf knockout mouse in the apolipoprotein E model.[15] In these studies mice specifically targeted for Arf, and shown to have no *Cdkn2b* compensation, did not display any change in lesion cellularity, aortic SMC proliferation, or SMC content. This suggests that *CDKN2B* itself may have a distinct role in SMC biology above and beyond the effects of ARF. Also, direct crosstalk between RB, MDM2, and p53 is known to exist in other cell types,[39,40] suggesting further investigation of direct interaction between *CDKN2B* and the kinases upstream of p53 in SMC.

This study has several limitations that warrant discussion. First, because this study used nonatherosclerotic models, it is difficult to draw inferences about a potential role for *CDKN2B* in coronary artery disease. The CAL model is useful to measure the response of SMC to injury but does not reflect human plaque formation. Also, Kim and colleagues,[41] recently reported that apolipoprotein E*Leiden/*CDKN2B* mice do not display an increase in atherosclerotic plaque burden relative to controls, raising the possibility that the 9p21-locus genes might have context-specific vascular effects, as has been described for p53 previously.[37] Indeed, it is possible that multiple cis-regulatory elements, compensation patterns, or gene-by-gene interactions may be active in different disease states with > 1 causal gene at 9p21.

In summary, this report provides a hypothesis for how variation at 9p21.3 may regulate SMC survival to promote risk for vascular disease. These findings highlight the concept of medial integrity as a determinant of disease progression and

rationalize the development of antiapoptotic therapies directed toward reducing aneurysm progression.

Acknowledgments

We gratefully acknowledge Linda Wolff of the National Cancer Institute at the National Institutes of Health for providing the *Cdkn2b* knockout mice and Jan Lindeman for providing human aortic sections used in this study.

Sources of Funding

This work was supported by National Institutes of Health grants R01HL103635 (to T.Q.), R01 HL38854 and R01 HL57353 (to G.K.O.), K12 HL087746 and K08 HL103605-01 (to N.J.L.), American Heart Association grant 10BGIA3290011 (to N.J.L.), and support from the LeDucq Foundation (to T.Q.).

Disclosures

None.

References

1. Lloyd-Jones DM, Nam BH, D'Agostino RB Sr, Levy D, Murabito JM, Wang TJ, Wilson PW, O'Donnell CJ. Parental cardiovascular disease as a risk factor for cardiovascular disease in middle-aged adults: a prospective study of parents and offspring. *JAMA*. 2004;291:2204–2211.
2. Marenberg ME, Risch N, Berkman LF, Floderus B, de Faire U. Genetic susceptibility to death from coronary heart disease in a study of twins. *N Engl J Med*. 1994;330:1041–1046.
3. Musunuru K, Kathiresan S. Genetics of coronary artery disease. *Annu Rev Genomics Hum Genet*. 2010;11:91–108.
4. Schunkert H, König IR, Kathiresan S, et al; Cardiogenics; CARDIoGRAM Consortium. Large-scale association analysis identifies 13 new susceptibility loci for coronary artery disease. *Nat Genet*. 2011;43:333–338.
5. Helgadottir A, Thorleifsson G, Manolescu A, et al. A common variant on chromosome 9p21 affects the risk of myocardial infarction. *Science*. 2007;316:1491–1493.
6. McPherson R, Pertsemlidis A, Kavaslar N, Stewart A, Roberts R, Cox DR, Hinds DA, Pennacchio LA, Tybjaerg-Hansen A, Folsom AR, Boerwinkle E, Hobbs HH, Cohen JC. A common allele on chromosome 9 associated with coronary heart disease. *Science*. 2007;316:1488–1491.
7. O'Donnell CJ, Kavousi M, Smith AV, et al; CARDIoGRAM Consortium. Genome-wide association study for coronary artery calcification with follow-up in myocardial infarction. *Circulation*. 2011;124:2855–2864.
8. Kathiresan S, Voight BF, Purcell S, et al; Myocardial Infarction Genetics Consortium; Wellcome Trust Case Control Consortium. Genome-wide association of early-onset myocardial infarction with single nucleotide polymorphisms and copy number variants. *Nat Genet*. 2009;41:334–341.
9. Cluett C, Tanaka T, Kisialiou A, Guralnik J, Ferrucci L, Frayling TM, Murray A, Melzer D. The rs1333049 snp near cdkn2a/2b, associated with myocardial infarction, is associated with increased risk of peripheral artery disease in older people. *Am Soc Hum Genet*. 2008;2:347–353
10. Matarin M, Brown WM, Singleton A, Hardy JA, Meschia JF; ISGS investigators. Whole genome analyses suggest ischemic stroke and heart disease share an association with polymorphisms on chromosome 9p21. *Stroke*. 2008;39:1586–1589.
11. Helgadottir A, Thorleifsson G, Magnusson KP, et al. The same sequence variant on 9p21 associates with myocardial infarction, abdominal aortic aneurysm and intracranial aneurysm. *Nat Genet*. 2008;40:217–224.
12. Bown MJ, Braund PS, Thompson J, London NJ, Samani NJ, Sayers RD. Association between the coronary artery disease risk locus on chromosome 9p21.3 and abdominal aortic aneurysm. *Circ Cardiovasc Genet*. 2008;1:39–42.
13. Gil J, Peters G. Regulation of the INK4b-ARF-INK4a tumour suppressor locus: all for one or one for all. *Nat Rev Mol Cell Biol*. 2006;7:667–677.
14. Krimpenfort P, Ijpenberg A, Song JY, van der Valk M, Nawijn M, Zevenhoven J, Berns A. p15Ink4b is a critical tumour suppressor in the absence of p16Ink4a. *Nature*. 2007;448:943–946.
15. González-Navarro H, Abu Nabah YN, Vinué A, Andrés-Manzano MJ, Collado M, Serrano M, Andrés V. p19(ARF) deficiency reduces macrophage and vascular smooth muscle cell apoptosis and aggravates atherosclerosis. *J Am Coll Cardiol*. 2010;55:2258–2268.
16. Kuo CL, Murphy AJ, Sayers S, Li R, Yvan-Charvet L, Davis JZ, Krishnamurthy J, Liu Y, Puig O, Sharpless NE, Tall AR, Welch CL. Cdkn2a is an atherosclerosis modifier locus that regulates monocyte/macrophage proliferation. *Arterioscler Thromb Vasc Biol*. 2011;31:2483–2492.
17. Liu Y, Sanoff HK, Cho H, Burd CE, Torrice C, Mohlke KL, Ibrahim JG, Thomas NE, Sharpless NE. INK4/ARF transcript expression is associated with chromosome 9p21 variants linked to atherosclerosis. *PLoS ONE*. 2009;4:e5027.
18. Pilbrow AP, Folkersen L, Pearson JF, et al. The chromosome 9p21.3 coronary heart disease risk allele is associated with altered gene expression in normal heart and vascular tissues. *PLoS ONE*. 2012;7:e39574.
19. Motterle A, Pu X, Wood H, Xiao Q, Gor S, Ng FL, Chan K, Cross F, Shohreh B, Poston RN, Tucker AT, Caulfield MJ, Ye S. Functional analyses of coronary artery disease associated variation on chromosome 9p21 in vascular smooth muscle cells. *Hum Mol Genet*. 2012;21:4021–4029.
20. Cunnington MS, Santibanez Koref M, Mayosi BM, Burn J, Keavney B. Chromosome 9p21 SNPs Associated with Multiple Disease Phenotypes Correlate with ANRIL Expression. *PLoS Genet*. 2010;6:e1000899.
21. Jarinova O, Stewart AF, Roberts R, Wells G, Lau P, Naing T, Buerki C, McLean BW, Cook RC, Parker JS, McPherson R. Functional analysis of the chromosome 9p21.3 coronary artery disease risk locus. *Arterioscler Thromb Vasc Biol*. 2009;29:1671–1677.
22. Ripatti S, Tikkanen E, Orho-Melander M, et al. A multilocus genetic risk score for coronary heart disease: case-control and prospective cohort analyses. *Lancet*. 2010;376:1393–1400.
23. Holdt LM, Beutner F, Scholz M, Gielen S, Gäbel G, Bergert H, Schuler G, Thiery J, Teupser D. ANRIL expression is associated with atherosclerosis risk at chromosome 9p21. *Arterioscler Thromb Vasc Biol*. 2010;30:620–627.
24. Holdt LM, Sass K, Gäbel G, Bergert H, Thiery J, Teupser D. Expression of Chr9p21 genes CDKN2B (p15(INK4b)), CDKN2A (p16(INK4a), p14(ARF)) and MTAP in human atherosclerotic plaque. *Atherosclerosis*. 2011;214:264–270.
25. Yu W, Gius D, Onyango P, Muldoon-Jacobs K, Karp J, Feinberg AP, Cui H. Epigenetic silencing of tumour suppressor gene p15 by its antisense RNA. *Nature*. 2008;451:202–206.
26. Kotake Y, Nakagawa T, Kitagawa K, Suzuki S, Liu N, Kitagawa M, Xiong Y. Long non-coding RNA ANRIL is required for the PRC2 recruitment to and silencing of p15(INK4B) tumor suppressor gene. *Oncogene*. 2011;30:1956–1962.
27. Harismendy O, Notani D, Song X, Rahim NG, Tanasa B, Heintzman N, Ren B, Fu XD, Topol EJ, Rosenfeld MG, Frazer KA. 9p21 DNA variants associated with coronary artery disease impair interferon-gamma signalling response. *Nature*. 2011;470:264–268.
28. Kral BG, Mathias RA, Suktitipat B, Ruczinski I, Vaidya D, Yanek LR, Quyyumi AA, Patel RS, Zafari AM, Vaccarino V, Hauser ER, Kraus WE, Becker LC, Becker DM. A common variant in the CDKN2B gene on chromosome 9p21 protects against coronary artery disease in Americans of African ancestry. *J Hum Genet*. 2011;56:224–229.
29. Minyard AN, Parker JC Jr. Intracranial saccular (berry) aneurysm: a brief overview. *South Med J*. 1997;90:672–677.
30. López-Candales A, Holmes DR, Liao S, Scott MJ, Wickline SA, Thompson RW. Decreased vascular smooth muscle cell density in medial degeneration of human abdominal aortic aneurysms. *Am J Pathol*. 1997;150:993–1007.
31. Kockx MM, De Meyer GR, Muhring J, Jacob W, Bult H, Herman AG. Apoptosis and related proteins in different stages of human atherosclerotic plaques. *Circulation*. 1998;97:2307–2315.
32. Libby P, Ridker PM, Maseri A. Inflammation and atherosclerosis. *Circulation*. 2002;105:1135–1143.
33. Kockx MM, Herman AG. Apoptosis in atherosclerosis: beneficial or detrimental? *Cardiovasc Res*. 2000;45:736–746.
34. Bies J, Sramko M, Fares J, Rosu-Myles M, Zhang S, Koller R, Wolff L. Myeloid-specific inactivation of p15Ink4b results in monocytosis and predisposition to myeloid leukemia. *Blood*. 2010;116:979–987.

35. Cunnington MS, Keavney B. Genetic mechanisms mediating atherosclerosis susceptibility at the chromosome 9p21 locus. *Curr Atheroscler Rep*. 2011;13:193–201.
36. Mayr U, Mayr M, Li C, Wernig F, Dietrich H, Hu Y, Xu Q. Loss of p53 accelerates neointimal lesions of vein bypass grafts in mice. *Circ Res*. 2002;90:197–204.
37. Sanz-González SM, Barquín L, García-Cao I, Roque M, González JM, Fuster JJ, Castells MT, Flores JM, Serrano M, Andrés V. Increased p53 gene dosage reduces neointimal thickening induced by mechanical injury but has no effect on native atherosclerosis. *Cardiovasc Res*. 2007;75:803–812.
38. Mercer J, Bennett M. The role of p53 in atherosclerosis. *Cell Cycle*. 2006;5:1907–1909.
39. Yap DB, Hsieh JK, Chan FS, Lu X. mdm2: a bridge over the two tumour suppressors, p53 and Rb. *Oncogene*. 1999;18:7681–7689.
40. Hsieh JK, Chan FS, O'Connor DJ, Mittnacht S, Zhong S, Lu X. RB regulates the stability and the apoptotic function of p53 via MDM2. *Mol Cell*. 1999;3:181–193.
41. Kim JB, Deluna A, Mungrue IN, Vu C, Pouldar D, Civelek M, Orozco L, Wu J, Wang X, Charugundla S, Castellani LW, Rusek M, Jakobowski H, Lusis AJ. Effect of 9p21.3 coronary artery disease locus neighboring genes on atherosclerosis in mice. *Circulation*. 2012;126:1896–1906.

SUPPLEMENT MATERIAL

Loss of *CDKN2B* promotes p53-dependent smooth muscle cell apoptosis and aneurysm formation

SUPPLEMENTAL METHODS

Murine models of vascular disease

The Cdkn2b$^{-/-}$ mice were the generous gift of Linda Wolff at the NIH/NCI[1]. These mice were generated by microinjection of 129SV/J ES cells into C57BL/6 blastocysts, which were then crossed with C57BL/6 mice to generate a congenic line with the targeted allele on a pure C57BL/6 background. All studies were approved by the Stanford University Administrative Panel on Laboratory Animal Care (protocols 10020, 10022) and conform to the Guide for the Care and Use of Laboratory Animals published by the US National Institutes of Health (NIH Publication No. 85-23, revised 1996). Baseline hemodynamic and metabolic analyses were performed by the Stanford Veterinary Service Center.

1.Murine AAA model

Porcine pancreatic elastase AAA infusion model

Animals used in the porcine pancreatic elastase (PPE) infusion study included 12-14 week old male: *Cdkn2b*$^{+/+}$ (n = 21) and*Cdkn2b*$^{-/-}$ (n = 24) mice on a C57BL/6 background[2]. Mice were anesthetized using 2.0–2.5% isoflurane (Vet One, Meridian, ID, USA) and a laparotomy was performed under sterile conditions, as previously described by our lab[3]. The abdominal aorta was isolated from the level of the renal vein to the bifurcation with the assistance of an operating stereomicroscope (Leica, Wetzlar, Germany). After placing temporary ligatures around the proximal and distal aorta, an aortotomy was created at the bifurcation with the tip of a 30-gauge needle. An insertion catheter was created by using a MicroRenathane Implantation tube (MRE010 and MRE025; Braintree Scientific Inc, Braintree, MA, USA) for infusion into the aorta. The catheter was introduced through the aortotomy, secured, and the aortic lumen was infused for 5 minutes at 100 mmHg with saline or saline containing type I porcine pancreatic elastase (1.5 U/mL; Sigma Aldrich, St. Louis, MO, USA). After removing the infusion catheter, the

aortotomy was repaired without constriction of the lumen. In some experiments, mice were injected with 2.2 mg/kg intraperitoneal pifithrin-α one day prior to ligation, and then every 48 hours until sacrifice, as previously described[4].

Aortic diameter measurements by ultrasound imaging

At baseline, and 3, 7 and 14 days after aneurysm induction, B-mode ultrasound (US) imaging was performed to assess the abdominal aortic diameter (AAD). Mice were anesthetized using 2% isoflurane (Vet One, Meridian, ID, USA), and laid supine on a heated 37°C plate. Two-dimensional B-mode imaging was performed using a real-time microvisualization scan head (RMV 704) with a central frequency of 40 MHz, frame rate of 30 Hz, a focal length of 6 mm, and a 20×20 mm field of view (Visualsonics, Toronto, Canada). Transverse image scans were performed and cine loops of 300 frames were acquired throughout the infra- and suprarenal region of the mouse aorta. The acquired images were stored digitally on a built-in hard drive for offline analysis to determine maximal AAD. All aortic diameters were measured in anterior-posterior direction during the diastolic phase. US image analysis was performed using the accompanying Vevo 770 software (Visualsonics, Toronto, Canada). Measurements were accomplished using random selection of each dataset and operator blinding to prevent recall bias. All measurements were collected by one observer to limit bias, while results were analyzed by a second independent observer blinded to the treatment group

Aortic tissue preparation, immunohistochemistry and lesion quantification

Mice were sacrificed at post-operative day 5 or 14 and perfused at a constant pressure of 100 mmHg through the heart with saline followed by warm (37°C) agarose gel (Amresco, Solon, OH, USA) diluted in saline (3% w/v). After the agarose solidified, the abdominal aorta was dissected free from the surrounding connective tissue and fixed in 4% formalin. Isolated tissue was then dehydrated through a graded sucrose series and subsequently embedded in OCT blocks. Aortic tissue was segmented into 7 *μ*m-thick serial sections from the left renal artery to the bifurcation and stained with Masson Trichrome (Sigma Aldrich, St. Louis, MO, USA), Picrosirius Red Stain (Polysciences, #24901),and Verhoeff Stain (Polysciences, # 25089) Kits. Additionally, sections were stained with primary antibodies against smooth

muscle α-actin (Abcam, 1:300), Mac-3 (BD Sciences BD 550292, 1:75), and CD-3 (Abcam, ab5690, 1:150). Biotinylated secondary antibodies followed by avidin-biotin-alkaline phosphatase substrate were used as previously described[5]. *In vivo* apoptosis was assessed by staining for TUNEL positivity with the Cell Death Detection Kit (Roche), per protocol. Cellular proliferation was measured by staining with PCNA (Abcam, ab2426, 1:500). The cellularity of the vessel was measured by manually counting nuclei of sections stained with DAPI. The Elastin Degradation Score was calculated as previously described[6]. Negative controls were performed with the omission of the primary antibody.

2. Murine carotid remodeling model

Carotid artery ligation model

Animals used in the carotid artery ligation (CAL) study included12-14 week old male: *Cdkn2b*$^{+/+}$(n = 64) and*Cdkn2b*$^{-/-}$ (n = 48) mice on a C57BL/6 background[2]. All animals underwent the endothelial-sparing complete carotid artery ligation as previously described[7]. This model does not reflect atherosclerosis or in-stent restenosis, but rather is a model used to study the response of the vascular SMC to injury[8]. Briefly, the right carotid arteries were dissected and completely ligated just proximal to the carotid bifurcation. In some experiments, mice were injected with 2.2 mg/kg intraperitoneal pifithrin-α one hour prior to ligation, and then every 48 hours until sacrifice, as previously described[4]. Animals were euthanized 2, 4, 7, 14 or 28 days after the surgery and both the ligated- and non-ligated carotid artery samples were harvested for either RNA, total protein, or histomorphometric analysis[5, 9].

Carotid tissue preparation, immunohistochemistry and lesion quantification

At sacrifice, the mice were perfused with PBS, and the carotids were dissected, fixed in 10% formalin and embedded in paraffin. Serial 5 µM sections were taken 400 µM, 800 µM, 1200 µM and 1600 µM proximal to the ligation site and stained with haematoxylin and eosin (DAKO) for morphometric analysis. Digitized images of the vessels were analyzed with Adobe Photoshop CS5. We measured the areas enclosed by the lumen, internal elastic lamina and external elastic lamina and then calculated the luminal area, neointimal area, medial area and total vessel area, as previously described[9].

Immunohistochemical staining was performed as described previously[9]. Briefly, sections were incubated with primary antibodies directed against smooth muscle α-actin (Abcam, 1:250) and then biotinylated secondary antibodies followed by avidin-biotin-alkaline phosphatase substrate reaction to detect SMC content[5]. *In vivo* apoptosis was assessed by staining for TUNEL positivity with the Cell Death Detection Kit (Roche), per protocol. Cellular proliferation was measured by staining with PCNA (Abcam, ab2426, 1:500). The cellularity of the vessel was measured by manually counting nuclei of sections stained with DAPI .

3. Bone Marrow Transplantation

Male C57BL/6 hosts received 10 Gy of total body irradiation (TBI) (200 Kv X-ray source) divided in 2 of 5Gy that were given in a 4h interval. Four hour after the last dose of TBI, hosts were received female C57BL/6 total bone marrow cells ($1x10^7$) by means of retro-orbital sinus injection. Animals were kept in autoclaved cages and received autoclaved food and antibiotics (sulfomethoxazole−trimethoprim, Schein Pharmaceutical) in water. Survival and body condition were monitored daily. Engraftment of donor cells was monitored in peripheral blood two weeks post-bone marrow transplantation as described 19180077. All stainings were performed in PBS/1% calf serum in the presence of purified anti-CD16/32 at saturation to block nonspecific staining via FcRII/III. Identification of T cells, B cells and monocytes were performed using PE-conjugated anti-CD3, APC-conjugated anti-B220, Pacific Blue-conjugated anti-F4/80 antibodies (All from BD Biosciences, San Jose, CA), respectively. All analyses were done using LSRII (Becton Dickinson) flow cytometer. FlowJo® software was used for data analysis.

Physiology studies

Systolic blood pressure, diastolic blood pressure and heart rate were recorded in conscious mice using a computerized, non-invasive tail cuff system (BP 2000 Blood Pressure Analysis System , Visitech Systems, Stratham, NH), as described previously[10, 11]. Mice were acclimatized to the apparatus during daily sessions over 6 days prior to data acquisition. Lipid analysis was performed in mice after an

overnight fast, as previously described[5]. In brief, total plasma cholesterol (CHOD-PAP; Roche Diagnostics), HDL (HDL-C-plus 2nd generation; Roche Diagnostics), and LDL concentrations (GPO-PAP; Roche Diagnostics) were measured using enzymatic kits on an automated analyzer (Roche) according to the manufacturer's instructions. Fasting glucose was measured in venous blood from a tail prick using a FreestyleGlucometer and glucose strips (Abbott).

Human vascular sample acquisition and preparation

Approval for studies on human tissue samples was obtained under informed consent and according to the declaration of Helsinki. Samples were obtained from two sources including Stanford University and the Leiden University Medical Center (LUMC) Biobank. For the Stanford cohort, human aortic samples were taken from patients during open surgical AAA repair (n =13), as well as from organ donors at the time of explant (n = 5). The patients undergoing surgery for enlarged abdominal aortas had aortic diameters of 57 to 68 mm. According to hospital documentation, all 13 patients were on similar medical therapy at the time of surgical intervention, including β-blockers, either angiotensin receptor blocker or angiotensin converting enzyme inhibitors, and statin therapy. All patients were male, of Caucasian descent, and non-diabetic. The control group was comprised of organ donor patients without AAA (*n* = 3 heart; *n* = 2 kidney) who were a mean age of 33 ± 33.4 years at the time of explantation. Samples were snap frozen and stored at -80°C. RNA was later extracted and analyzed, as described below.

Samples from the LUMC Biobank were a generous gift of Dr. Jan Lindeman. These samples were harvested from cadaveric donors (n = 7) or patients undergoing AAA surgery (n = 7), as previously described[12, 13]. All samples were obtained in accordance with the guidelines of the Medical Ethical Committee of the Leiden University Medical Center and the code of conduct of the Dutch Federation of Biomedical Scientific Societies (http://www.federa.org/gedragscodes-codes-conduct-en). These samples were fixed in formaldehyde (24 hours), decalcified (Kristensen's solution, 120 hours), and paraffin embedded for histological analysis, as previously described[14]. Immunohistochemical staining was performed as described previously[5, 9]. Briefly, after deparaffinization and decloaking, sections were incubated with primary antibodies directed against smooth muscle α-actin (Abcam, ab5694, 1:250), von

Willebrand's Factor (Abcam, ab6994, 1:250) or CDKN2B (Santa Cruz, sc-613, 1:25). Colorimetric secondary antibodies included Rabbit-on-Rodent AP-Polymer (Biocare Medical) followed by a substrate reaction with Vulcan Fast Red Chromagen Kit 2 (Biocare Medical). Immunoflourescent staining was performed with Alexa Fluor 594 goat anti-rabbit antibody (1:500).

Cell culture methods

Human coronary artery, pulmonary artery and aortic SMC(Lonza, Walkersville, MD, passage #3-6) were propagated in SmGM-2 growth media (Lonza) containing 5% FBS. Human coronary artery endothelial cells (HCAEC) and pulmonary artery endothelial cells (HPAEC) (Lonza) were grown in EGM-growth media containing 10% FBS. RAW 264.7 macrophages (ATCC) were grown in DMEM-growth media containing 10% FBS. NIH/3T3 fibroblasts were grown in DMEM-growth media containing 10% FBS. To induce growth arrest and the expression of differentiation genes, SMC were serum starved in basal media (SmBM) for 72 hours, according to conventional protocols[15, 16]. *In vitro P53* inhibition studies were completed by adding 10uM pifithrin-α (Calbiochem) to the cell culture media, as previously described[17]. All physiology experiments were performed in both HCASMC and AoSMC. Subsequent protein array and Western blot studies were restricted to HCASMC.

For knockdown experiments, SMC were transfected with 300 nM of anti-*CDKN2B*, anti-*CDKN2A* or high-GC negative control siRNA (Ambion, Silencer Select, catalog # 4390825, 4390824 and 4390843, respectively) using the high-efficiency Amaxa Nucleofector system (Lonza, protocol U-025). Successful transfection (> 85% of all cells) was confirmed by visual fluorescent microscopic analysis and fluorescence activated cell sorting (FACS) flow cytometry for the fluorescently-labeled positive control, pmax GFP (Amaxa). Plates were harvested at 80% confluence for RNA and protein analysis or used for subsequent *in vitro* analysis. Reproducible knockdown of *CDKN2B* was confirmed in SMC by quantitative rt-PCR which displayed selective silencing of this gene on the order of ~85%. No off target knockdown was observed for any of the other C9CAR genes, including CDKN2A, ARF or ANRIL.

mRNA isolation and quantitative reverse-transcription PCR

RNA was isolated from cell lysates using the miRNeasy Mini Kit (Qiagen, Valencia, CA) according to the manufacturer's protocol. RNA was isolated from the murine and human vascular samples using the Trizol method (Invitrogen). RNA was quantified with the Nanodrop machine (Agilent Technologies, Santa Clara, CA)For quantitation of gene transcription, cDNA was generated with M-MuLV reverse transcriptase, and then amplified on the ABI PRISM 7900HT with commercially available TaqMan primers (Applied Biosystems, Foster City, CA) and normalized to 18S internal controls, as previously described[16]. A list of the primers and probes used in these studies is provided in Table 1 below.

Western blot analysis

Total protein was isolated from snap frozen vascular and experimental cell culture samples in lysis buffer (NP-40) with protease/phosphatase inhibitors (Roche) and PMSF, as previously described[16]. 20 µg of cellular lysate from each sample was subjected to Western blotting with rabbit α-human p-53 (1:200, SCBT, sc-6243), mouse α-human pRb (1:250, BDPharmingen, 554136), rabbit α-human p21 (1:200, SCBT, sc-397), rabbit α-human BAX(1:200, SCBT, sc-6236), rabbit α-human BCL-2 (1:200, SCBT, sc-783), mouse α-human SMP14 mdm2 (1:100, SCBT, sc-965), mouse α-human 2A10 mdm2 (4µg/mL, Abcam, ab16895), rabbit α-human/mouse/rat phospho serine 166 mdm2 (1:250, Cell Signaling, #3521) primary antibodies, and then HRP-conjugated goat α-mouse (1:1500, Invitrogen) or goat α-rabbit (1:2000, Invitrogen) secondary antibodies, as appropriate. Rabbit α- human GAPDH (1:2000) primary antibody was used as an internal loading control. Exposed films were scanned, and integrated band densities were obtained and analyzed with ImageJ software in a blinded fashion, and normalized to GAPDH content for each sample, as previously described[16].

Cell culture assays

Cell cycle analysis and cellular proliferation assays

A modified MTT (3-[4,5-dimethyl-thiazol-2-yl]-2,5-diphenyltetrazolium bromide) assay was performed to analyze SMC proliferation and viability, as previously described[16]. Transfected HCASMC were grown in 96-well plates for 24-36 hours and then incubated for 4 hours in the presence of 10 µL of MTT AB

solution (Millipore, Billerica, MA). The formazan product was dissolved by addition of 100 µL acidic isopropanol (0.04 N HCl) and absorbance was measured at 570 nm (reference wavelength 630 nm) on an ELISA plate reader. For cell counting assays, HCASMC were transfected with siRNA for CDKN2B or an siRNA control. Cells were then harvested by trypsinization after 72 hours of serum starvation, and viable cell counts were obtained by hemocytometer and trypan blue exclusion. Additionally, cell cycle quantification was performed by FACS analysis, as previously described[11]. Briefly, cell suspensions containing $1x10^6$ transfected HCASMC were fixed in 70% ethanol, centrifuged for 5 minutes at 4^o C, then resuspended in PBS containing propidium iodide (10 µg/ml; Sigma) and RNase A (10 µg/ml; Sigma) prior to analysis by FACS (FACSCalibur; BD Biosciences).

Boyden chamber chemotaxis assays

To analyze SMC migration, a modified Boyden chamber assay was performed, as previously described[9]. Briefly, 6-well trans-well migration chambers with 8 µm pores (Becton Dickinson) were employed. Transfected human HCASMC ($5x10^4$ cells/well) were serum starved in SmBM for 72 hours and then plated in the upper chamber in 1 mL of SmBM. Two mL of SmGM-2 media were added to the lower chamber, and the cells were allowed to migrate for 24 hours at 37 °C. Cells that migrated to the lower chamber were fixed in methanol, stained with 0.1% crystal violet and manually counted in a blinded fashion (8 high-power fields/well).

Apoptosis assays

Rates of programmed cell death were assessed with three independent *in vitro* assays. In each assay, $1x10^5$ transfected HCASMC were treated with 1 µM staurosporine (Sigma, S5921) in serum free media for 6 hours prior to analysis. In the first assay, caspase-3 and -7 activity was measured using a commercially available luminometric assay (Promega, G-8093), according to the manufacturer's protocol. In the second assay, the cells were harvested in TrypLE (Life Sciences) and stained with 10 µL FITC annexin V and 10 µL propidium iodide (BD Pharmingen) and FACS sorted within one hour (BD FACSCaliber, 530 nm [FL1] and >575 nm [FL3]). Analysis was performed with FloJo 7.6.3. In the final

assay, the cells were plated onto 4-well chamber slides (Lab-Tek II, 154526), then fixed in 10% formalin for 30 minutes prior to TUNEL staining with the Cell Death Detection Kit (Roche). The slides were photographed at 20x magnification and analyzed for percentage of cells undergoing apoptosis (normalized to total cells per high power field (hpf) as assessed by DAPI counterstain (Vector).

Phospho-proteomic analysis

The phosho-proteomic profile of apoptosing CDKN2B-deficient cells was compared to apoptosing control transfected cells using the p53 Signaling Phospho Antibody Microarray (Full Moon BioSystems), according to the manufacturer's protocol. The arrays were scanned on the GenePix4000B Microarray Scanner (Molecular Diagnostics) and analyzed with the provided GAL file. Significantly regulated proteins were identified by Statistical Analysis of Microarrays (SAM) and confirmed with Western blotting and flow cytometry. Pathway enrichment analysis for genes representing differentially regulated proteins at FDR < 1% were identified using DAVID bioinformatics analysis ($p<0.05$) (NCBI).

Statistical analysis

Data are presented as mean± SEM. Data were subjected to the Kolmogorov-Smirnov test to determine distribution. Groups were compared using the Mann-Whitney U test for non-parametric data or the Students t-test for parametric data. When comparing multiple groups, data were analyzed by analysis of variance with Bonferroni'spost test. For multiple testing of parametric data, a value of $P<0.05$ was considered statistically significant. Experiments were replicated at least in quadruplicate and all analyses were performed in a blinded fashion by two separate investigators, unless otherwise specified. Statistical analysis was performed with GraphPad Prism 5.

SUPPLEMENTAL FIGURES

Supplemental Figure I. *Cdkn2b* does not alter any metabolic or hemodynamic parameters in vivo. Compared to wild type mice (grey bars) **.** *Cdkn2b*$^{-/-}$ mice (black bars) displayed no difference in invasively measured heart rate, or blood pressure (n = 7 per group). Similarly, no difference in any lipid parameter or fasting glucose was observed across genotypes (n=4-7 per experiment). No tumors were observed in any of the mice in this study.

Supplemental Figure II. Bone marrow recipients showed signs of hematopoietic reconstitution 2 weeks post-transplantation. Following red blood cell lysis, staining of B cells (B220), T cells (CD3) and monocytes (F4/80) was performed using fluorochrome-conjugated antibodies. Successful reconstitution of B cells, T cells and monocytes (F4/80) was detected in peripheral blood of *Cdkn2b* knockout mice reconstituted with bone marrow from wild type mice (KOxWT), wild type reconstituted with *Cdkn2b* knockout (WTxKO), wild type reconstituted with wild type (WTxWT). Non-irradiated wild type mice were included in the analysis as control (WT). (A). Representative contour plots demonstrating phenotypic characterization of $CD3^-B220^+$ B cells, $CD3^+B220^-$ T cells, and $CD3^-B220^-F4/80^+$ monocytes in hosts' peripheral blood (B). n = 15 mice for each condition.

Supplemental Figure III. *CDKN2B* is downregulated in vascular disease states and localizes to the medial layer. (A) *CDKN2B* mRNA levels were significantly reduced in human AAA tissues compared to normal aortic tissue*s* (4.8 fold reduction, $P<0.02$). *Cdkn2b* expression was downregulated 3-fold in the ligated mouse carotid artery relative to the uninjured vessel 14 days post carotid ligation (n =7). *CDKN2B* expression is downregulated 7.2 fold in human coronary artery SMC undergoing dedifferentiation in response to serum feeding. (B) *CDKN2B* immunolocalization revealed easily detectable protein expression in medial cells, but diminished immunostaining in the media of aneurysmal vessels. (C) Immunolocalization of *CDKN2B* with smooth muscle α-actin (SMA) indicates expression in vascular SMC. There is minimal colocalization of *CDKN2B* expression with the endothelial marker vWF. * = $P < 0.05$; + = $P < 0.03$; # = $P < 0.01$; ** = $P < 0.001$.

Supplemental Figure IV. *CDKN2B* does not regulate SMC differentiation. Compared to control-transfected cells (grey bars), siRNA directed against *CDKN2B* (black bars) induced effective knockdown with no off-target effects on other 9p21 locus genes. Knockdown of *CDKN2B* had no measurable effect on the differentiation status of HCASMC, as measured by the expression of SMC-differentiation genes SMA-actin, myosin heavy chain and transgellin. **.**

Supplemental Figure V. Putative mechanism for the interactions of the cyclin-dependent kinase inhibitors with factors that regulate the balance and kinetics of cell-cycling and cellular apoptosis. Known interactions are represented by solid lines and additional possible interactions represented by dashed lines.

Supplemental Table I. Genotyping primers and PCR probes used in this study.

Primer	Sequence
Mouse genotyping primer	
Cdkn2b WT Forward	CACGGAGCAGAACCCAACT
Cdkn2b WT Reverse	TGCAGATACCTCGCAATGTC
Cdkn2b KO Forward	ATCCGAGTGCCTACACCTCCA
Cdkn2b KO Reverse	GCTCCCGATTCGCAGCGCAT
Mouse Probes	ABI catalog number
Cdkn2b	Mm00483241_m1
p16Ink4a	Mm00494449_m1
p19Arf	Mm01257348_m1
MTAP	Mm01257902_m1
Human Probes	ABI catalog number
CDKN2B	Hs00793225_m1
CDKN2A	Hs99999189_m1
p14/ARF	Hs00923894_m1
ANRIL	Hs01390879_m1
MTAP	Hs00559618_m1
p53	Hs00153340_m1
p21	Hs00153277_m1
RB	Hs01078066_m1
SMA ACTIN	Hs00426835_g1
MYOSIN HEAVY CHAIN	Hs00224610_m1
TRANSGELLIN	Hs00162558_m1

1. Wolff L, Garin MT, Koller R, Bies J, Liao W, Malumbres M, Tessarollo L, Powell D, Perella C. Hypermethylation of the ink4b locus in murine myeloid leukemia and increased susceptibility to leukemia in p15(ink4b)-deficient mice. *Oncogene*. 2003;22:9265-9274
2. Rosu-Myles M, Taylor BJ, Wolff L. Loss of the tumor suppressor p15ink4b enhances myeloid progenitor formation from common myeloid progenitors. *Exp Hematol*. 2007;35:394-406
3. Leeper NJ, Tedesco MM, Kojima Y, Schultz GM, Kundu RK, Ashley EA, Tsao PS, Dalman RL, Quertermous T. Apelin prevents aortic aneurysm formation by inhibiting macrophage inflammation. *Am J Physiol Heart Circ Physiol*. 2009;296:H1329-1335
4. Li J, Ghiani CA, Kim JY, Liu A, Sandoval J, DeVellis J, Casaccia-Bonnefil P. Inhibition of p53 transcriptional activity: A potential target for future development of therapeutic strategies for primary demyelination. *J Neurosci*. 2008;28:6118-6127
5. Chun HJ, Ali ZA, Kojima Y, Kundu RK, Sheikh AY, Agrawal R, Zheng L, Leeper NJ, Pearl NE, Patterson AJ, Anderson JP, Tsao PS, Lenardo MJ, Ashley EA, Quertermous T. Apelin signaling antagonizes ang ii effects in mouse models of atherosclerosis. *J Clin Invest*. 2008;118:3343-3354
6. Sun J, Sukhova GK, Yang M, Wolters PJ, MacFarlane LA, Libby P, Sun C, Zhang Y, Liu J, Ennis TL, Knispel R, Xiong W, Thompson RW, Baxter BT, Shi GP. Mast cells modulate the pathogenesis of elastase-induced abdominal aortic aneurysms in mice. *J Clin Invest*. 2007;117:3359-3368
7. Harmon KJ, Couper LL, Lindner V. Strain-dependent vascular remodeling phenotypes in inbred mice. *Am J Pathol*. 2000;156:1741-1748
8. Xu Q. Mouse models of arteriosclerosis: From arterial injuries to vascular grafts. *Am J Pathol*. 2004;165:1-10
9. Kojima Y, Kundu RK, Cox CM, Leeper NJ, Anderson JA, Chun HJ, Ali ZA, Ashley EA, Krieg PA, Quertermous T. Upregulation of the apelin-apj pathway promotes neointima formation in the carotid ligation model in mouse. *Cardiovasc Res*. 2010;87:156-165
10. Krege JH, Hodgin JB, Hagaman JR, Smithies O. A noninvasive computerized tail-cuff system for measuring blood pressure in mice. *Hypertension*. 1995;25:1111-1115
11. Charo DN, Ho M, Fajardo G, Kawana M, Kundu RK, Sheikh AY, Finsterbach TP, Leeper NJ, Ernst KV, Chen MM, Ho YD, Chun HJ, Bernstein D, Ashley EA, Quertermous T. Endogenous regulation of cardiovascular function by apelin-apj. *Am J Physiol Heart Circ Physiol*. 2009;297:H1904-1913
12. van Dijk RA, Virmani R, von der Thusen JH, Schaapherder AF, Lindeman JH. The natural history of aortic atherosclerosis: A systematic histopathological evaluation of the peri-renal region. *Atherosclerosis*. 2010;210:100-106
13. Verschuren L, Lindeman JH, van Bockel JH, Abdul-Hussien H, Kooistra T, Kleemann R. Up-regulation and coexpression of mif and matrix metalloproteinases in human abdominal aortic aneurysms. *Antioxid Redox Signal*. 2005;7:1195-1202
14. Lindeman JH, Abdul-Hussien H, van Bockel JH, Wolterbeek R, Kleemann R. Clinical trial of doxycycline for matrix metalloproteinase-9 inhibition in patients with an abdominal aneurysm: Doxycycline selectively depletes aortic wall neutrophils and cytotoxic t cells. *Circulation*. 2009;119:2209-2216
15. Owens GK, Loeb A, Gordon D, Thompson MM. Expression of smooth muscle-specific alpha-isoactin in cultured vascular smooth muscle cells: Relationship between growth and cytodifferentiation. *J Cell Biol*. 1986;102:343-352
16. Leeper NJ, Raiesdana A, Kojima Y, Chun HJ, Azuma J, Maegdefessel L, Kundu RK, Quertermous T, Tsao PS, Spin JM. Microrna-26a is a novel regulator of vascular smooth muscle cell function. *J Cell Physiol*. 2011;226:1035-1043
17. Chan KC, Wang CJ, Ho HH, Chen HM, Huang CN. Simvastatin inhibits cell cycle progression in glucose-stimulated proliferation of aortic vascular smooth muscle cells by up-regulating cyclin dependent kinase inhibitors and p53. *Pharmacol Res*. 2008;58:247-256

Suppl Fig I

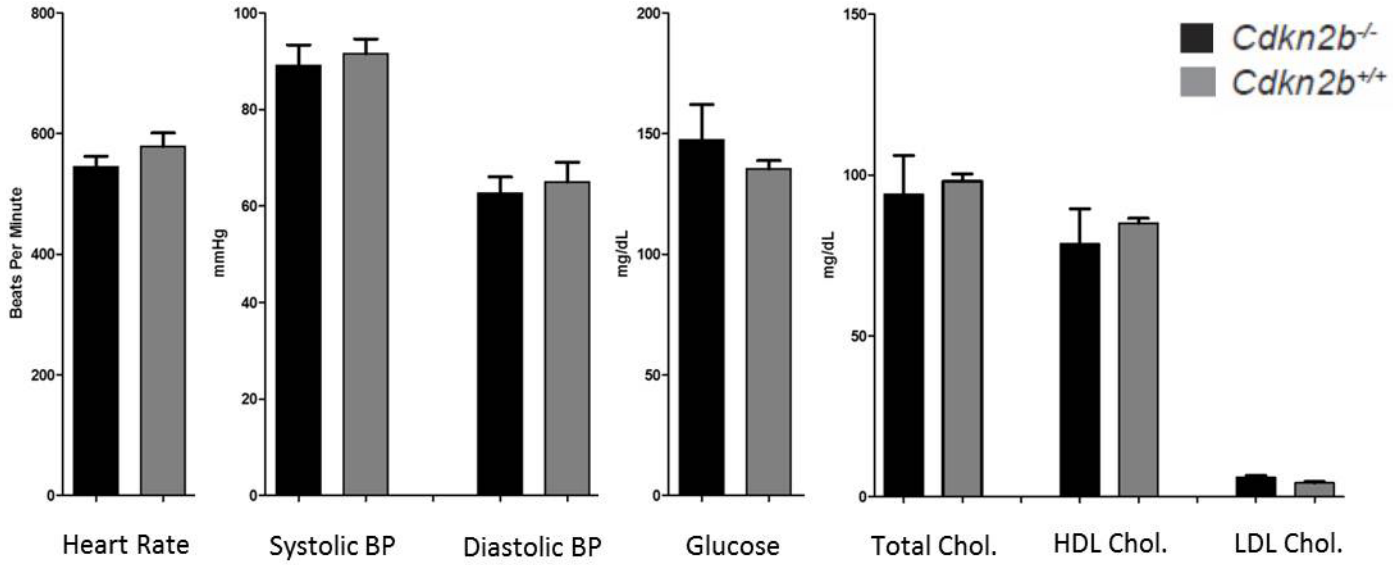

Suppl Fig II

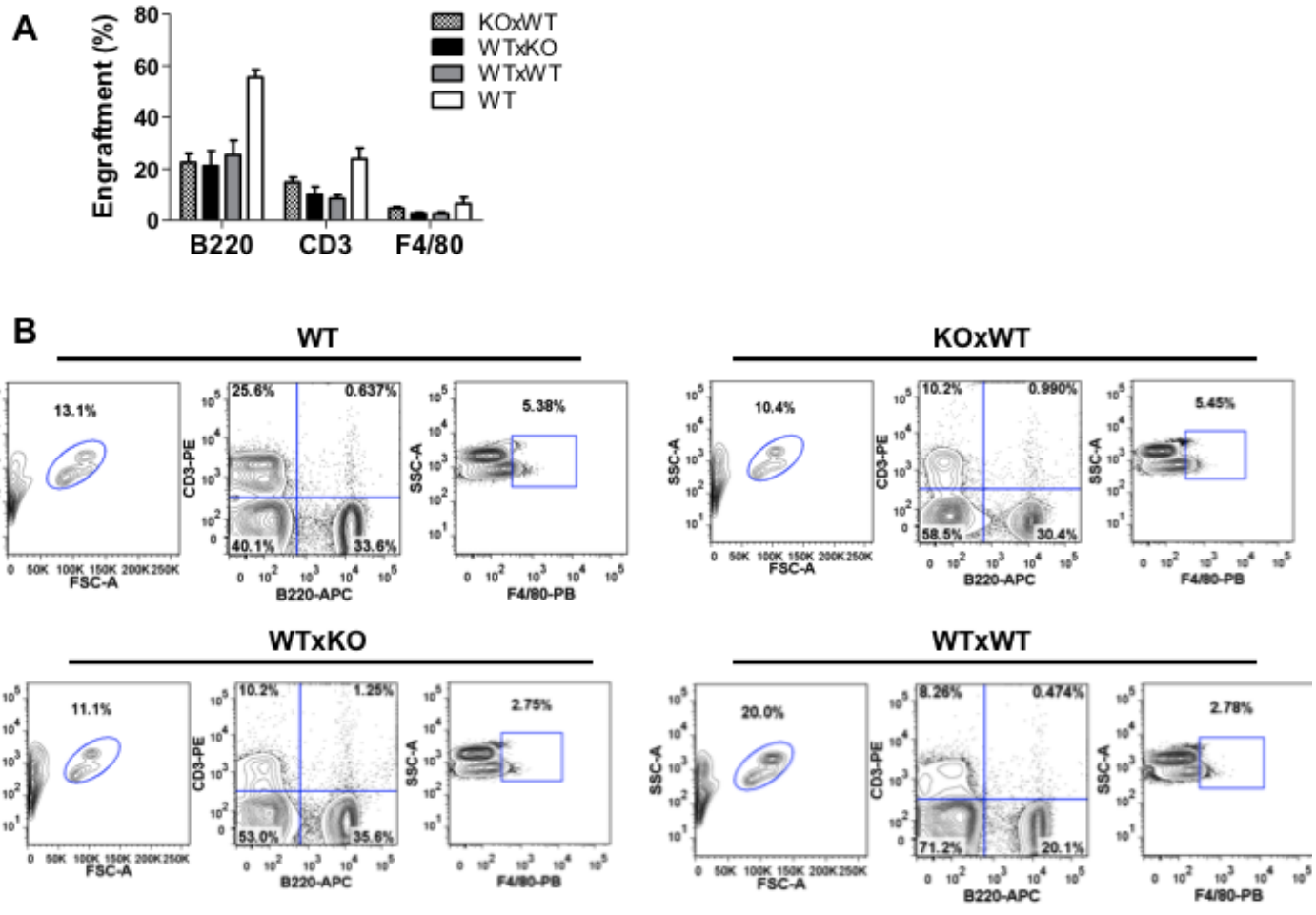

Suppl Fig III

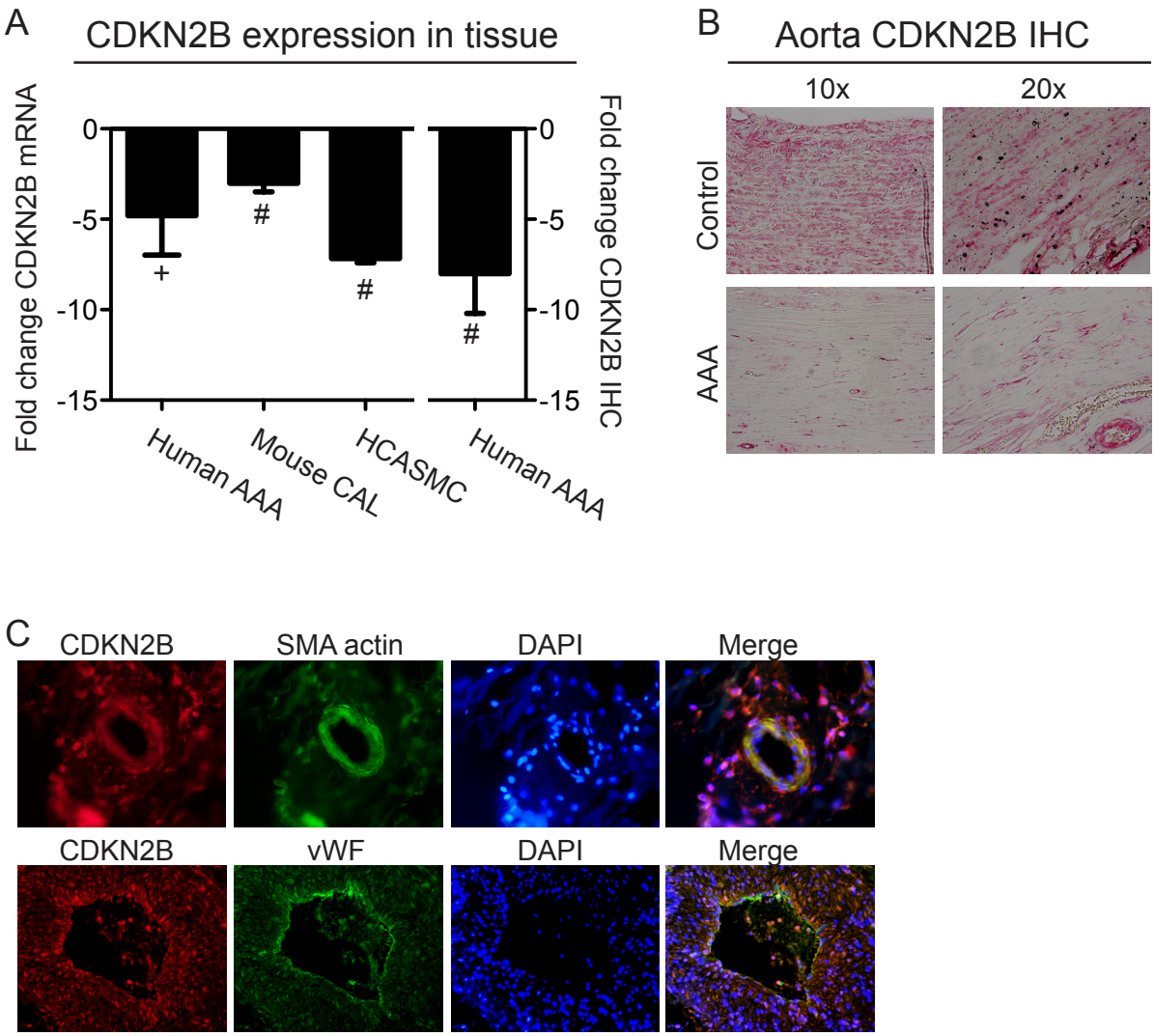

Suppl Fig IV

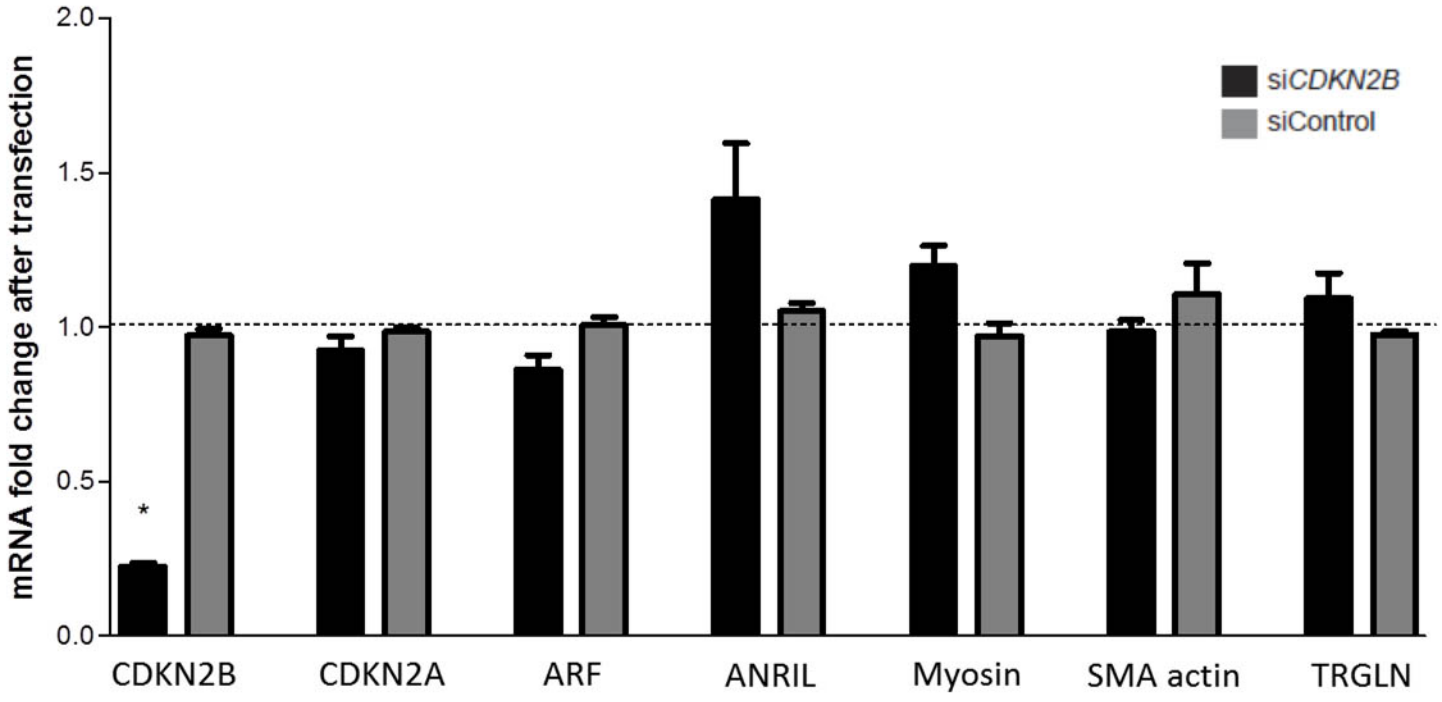

Suppl Fig.V